International Journal on Advances in Networks and Services

2022 vol. 15 nr. 1&2

The *International Journal on Advances in Networks and Services* is published by IARIA.
ISSN: 1942-2644
journals site: http://www.iariajournals.org
contact: petre@iaria.org

Sponsored by IARIA
www.iaria.org

International Journal on Advances in Networks and Services
Volume 15, Number 1 & 2, 2022

Christos Bouras, University of Patras, Greece
Mahmoud Brahimi, University of Msila, Algeria
Marco Bruti, Telecom Italia Sparkle S.p.A., Italy
Dumitru Burdescu, University of Craiova, Romania
Diletta Romana Cacciagrano, University of Camerino, Italy
Maria-Dolores Cano, Universidad Politécnica de Cartagena, Spain
Juan-Vicente Capella-Hernández, Universitat Politècnica de València, Spain
Eduardo Cerqueira, Federal University of Para, Brazil
Bruno Chatras, Orange Labs, France
Marc Cheboldaeff, Deloitte Consulting GmbH, Germany
Kong Cheng, Vencore Labs, USA
Dickson Chiu, Dickson Computer Systems, Hong Kong
Andrzej Chydzinski, Silesian University of Technology, Poland
Hugo Coll Ferri, Polytechnic University of Valencia, Spain
Noelia Correia, University of the Algarve, Portugal
Noël Crespi, Institut Telecom, Telecom SudParis, France
Paulo da Fonseca Pinto, Universidade Nova de Lisboa, Portugal
Orhan Dagdeviren, International Computer Institute/Ege University, Turkey
Philip Davies, Bournemouth and Poole College / Bournemouth University, UK
Carlton Davis, École Polytechnique de Montréal, Canada
Claudio de Castro Monteiro, Federal Institute of Education, Science and Technology of Tocantins, Brazil
João Henrique de Souza Pereira, University of São Paulo, Brazil
Javier Del Ser, Tecnalia Research & Innovation, Spain
Behnam Dezfouli, Universiti Teknologi Malaysia (UTM), Malaysia
Daniela Dragomirescu, LAAS-CNRS, University of Toulouse, France
Jean-Michel Dricot, Université Libre de Bruxelles, Belgium
Wan Du, Nanyang Technological University (NTU), Singapore
Matthias Ehmann, Universität Bayreuth, Germany
Wael M El-Medany, University Of Bahrain, Bahrain
Imad H. Elhajj, American University of Beirut, Lebanon
Gledson Elias, Federal University of Paraíba, Brazil
Rainer Falk, Siemens AG - Corporate Technology, Germany
Károly Farkas, Budapest University of Technology and Economics, Hungary
Huei-Wen Ferng, National Taiwan University of Science and Technology - Taipei, Taiwan
Gianluigi Ferrari, University of Parma, Italy
Mário F. S. Ferreira, University of Aveiro, Portugal
Bruno Filipe Marques, Polytechnic Institute of Viseu, Portugal
Ulrich Flegel, HFT Stuttgart, Germany
Juan J. Flores, Universidad Michoacana, Mexico
Ingo Friese, Deutsche Telekom AG - Berlin, Germany
Sebastian Fudickar, University of Potsdam, Germany
Stefania Galizia, Innova S.p.A., Italy
Ivan Ganchev, University of Limerick, Ireland / University of Plovdiv “Paisii Hilendarski”, Bulgaria
Miguel Garcia, Universitat Politecnica de Valencia, Spain
Emiliano Garcia-Palacios, Queens University Belfast, UK
Marc Gilg, University of Haute-Alsace, France

Wenbing Zhao, Cleveland State University, USA
Zibin Zheng, The Chinese University of Hong Kong, China
Yongxin Zhu, Shanghai Jiao Tong University, China
Zuqing Zhu, University of Science and Technology of China, China
Martin Zimmermann, University of Applied Sciences Offenburg, Germany

International Journal on Advances in Networks and Services
Volume 15, Numbers 1 & 2, 2022

CONTENTS

Licensed Millimeter-Wave Spectrum Allocation and Reuse in Indoor Environments

Rony Kumer Saha
Department of Electrical and Electronic Engineering, School of Engineering
BRAC University
66 Mohakhali, Dhaka 1212, Bangladesh
Email: rony.saha@bracu.ac.bd

***Abstract*—In this paper, by exploiting the frequency domain, we propose a Countrywide Millimeter-Wave (mmWave) Spectrum Allocation and Reuse (CoMSAR) technique that allocates and reuses spatially the countrywide 28 GHz spectrum to each Mobile Network Operator (MNO) of a country to operate its small cells per floor in a building. An interference management scheme is developed to avoid Co-Channel Interference (CCI) in each apartment. We model user statistics per small cell and interferer statistics per apartment and formulate the optimal amount of spectrum for each MNO. We derive average capacity, Spectral Efficiency (SE), Energy Efficiency (EE), and Cost Efficiency (CE) for the proposed technique and the traditional Static Licensed Spectrum Allocation (SLSA) technique allocating an equal amount of spectrum to each MNO. By varying CCI and spectrum reuse, extensive numerical and simulation results and analyses are carried out for a country consisting of four MNOs, i.e., MNOs 1, 2, 3, and 4 with a subscriber base of, respectively, 40%, 30%, 20%, and 10% of the countrywide subscribers. It is shown that CoMSAR with no CCI provides 2.5 times higher average capacity, SE, EE, and CE than that with the maximum CCI. However, with regard to SLSA, it improves the average capacity, SE, EE, and CE of MNO 1 by 300%, 165%, 75%, and 60%, respectively, with no CCI, each of which decreases to the minimum value when CCI is the maximum. Further, we show that CoMSAR can satisfy SE and EE requirements for sixth-generation (6G) mobile systems by reusing the countrywide 28 GHz spectrum to small cells of MNO 1 of about 61.2% less number of single-floor buildings with no CCI, whereas 6.4% less number of single-floor buildings with the maximum CCI, than that required by SLSA. Finally, we discuss the benefits and point out key issues of CoMSAR for further studies.**

***Keywords*—6G; 28 GHz; countrywide; millimeter-wave; mobile network; spectrum allocation; spectrum reuse; indoor; small cell.**

I. INTRODUCTION

A. Background

The high capacity and data rate requirements for the existing mobile networks impose a demand for the massive radio spectrum availability on a Mobile Network Operator (MNO). Due to this reason, the traditional model (Foster [2] for allocating a portion of the licensed spectrum statically in an exclusive manner for a long time has no longer been considered effective to address the ever-increasing high capacity and data rate demands. Though these requirements have been increased over time, the availability of the spectrum for an MNO has not increased correspondingly, resulting in the scarcity of the radio spectrum. In this regard, spectrum allocation and spectrum exploitation can play a vital role in addressing the spectrum scarcity for an MNO in a country. Spectrum allocation techniques describe how the spectrum specified for a country is allocated to its MNOs. The usefulness of a spectrum allocation technique is affected by factors, such as the amount and duration of the allocated spectrum to an MNO, as well as the user traffic demand of an MNO (Saha [3]). By carefully allocating the spectrum specified for a country among its MNOs, the available amount of spectrum for an MNO can be extended considerably. Furthermore, by exploiting the available spectrum for an MNO in space, for example, the utilization of the spectrum can be increased. Accordingly, the spatial reuse of the spectrum to small cells, particularly in a 3-Dimensional (3D) space, e.g., a multistory building, is considered an effective approach to increase the utilization of the available spectrum.

B. Related Work

Numerous research works have already addressed the issues of spectrum allocation, as well as spectrum exploitation. For example, Yan et al. [4] have proposed methods for the dynamic spectrum allocation in cognitive radio systems, and Wei et al. [5] have presented a system-level dynamic frequency spectrum allocation scheme based on central heterogeneous network architecture. Using the carrier aggregation technique, Shajaiah et al. [6] have considered the optimization of resource allocation, whereas, based on the access mechanism, Liu et al. [7] have proposed a joint subcarrier and power allocation method. Further, Kim et al. [8] have introduced the functionalities required for entities related to the spectrum allocation to propose a spectrum allocation algorithm in multiple network operators' scenarios. Moreover, Kim et al. [9] have introduced and formulated the problem of the optimum spectrum allocation in cognitive radios. Furthermore, Gu [10] has proposed a new dynamic spectrum allocation algorithm to resolve channel conflict problems in channel switching and Bhuiyan et al. [11] have developed a traffic-load-aware channel allocation mechanism for secondary users.

Regarding the spectrum exploitation by means of reusing the available spectrum, an analytical model has been proposed by Saha and Aswakul [12] to reuse the microwave spectrum, as well as by Saha [13] to reuse the 28 GHz millimeter-wave (mmWave) spectrum, in a 3D building of small cells. Likewise, Saquib et al. [14] have investigated a number of Fractional Frequency Reuse (FFR) schemes, whereas Hasan et al. [15] have proposed the dynamic fractional frequency reuse (DFFR) method to reduce the inter-cell interference. Moreover, Saha [16] has proposed a technique to reuse the same spectrum for small cells deployed in a building by forming 3D clusters of small cells. Besides, in time-varying channels, Yen et al. [17] have developed new FFR patterns for multi-cell orthogonal frequency-division multiple access systems with frequency or time division duplexing (FDD/TDD). Further, Lam et al. [18] have presented the performance of well-known frequency reuse algorithms in terms of, e.g., system throughput and average packet loss ratio.

C. Problem Statement and Contribution

However, unlike the traditional static licensed spectrum allocation that considers allocating a certain portion of the countrywide spectrum to an MNO, the whole countrywide mmWave spectrum can be allocated to each MNO to increase its spectrum. Besides, due to the high floor penetration loss, the same countrywide mmWave spectrum for each MNO can be exploited spatially on the inter-floor level to reuse more than once by small cells within a building. Hence, a technique that can employ both the spectrum allocation and spectrum exploitation means to the mmWave spectrum using in-building small cells to allocate the countrywide mmWave spectrum to each MNO, which is exploited further to be spatially reused by small cells in a building is considered promising to achieve high Spectral Efficiency (SE) and Energy Efficiency (EE) requirements for the next generation mobile networks.

Numerous studies have already attempted to achieve the expected SE and EE requirements for the Sixth-Generation (6G) mobile networks by employing the mmWave spectrum allocation and exploitation. For example, by exploiting the power domain, Saha [19] has proposed a hybrid interweave-underlay spectrum access and reuse technique to address the dynamic spectrum access and reuse of the countrywide 28 GHz mmWave spectrum to in-building small cells of each MNO in a country to achieve the required SE and EE of 6G. Unlike the countrywide mmWave spectrum, by exploiting the secondary spectrum trading, Saha [20] has proposed a dynamic exclusive-use spectrum access method to share partly and exclusively the licensed mmWave spectrum of one MNO to another in a country to address the SE and EE requirements for 6G. Further, Saha [21] has presented a technique for the 3D spatial reuse of 28 and 60 GHz mmWave spectra allocated to an MNO to its in-building small cells to achieve the expected SE and EE requirements for 6G networks. Unlike these existing literature works, in this paper, by exploiting the frequency domain, we propose A Countrywide MmWave Spectrum Allocation and Reuse (CoMSAR) technique that considers allocating and then reusing the massive 28 GHz mmWave spectrum specified countrywide to each MNO of a country to operate its small cells deployed on each floor in a multistory building to achieve the expected SE and EE requirements for 6G mobile networks.

D. Organization

In addressing the proposed technique, we first present the system architecture and the proposed technique, as well as develop a frequency-domain Co-Channel Interference (CCI) avoidance scheme, in Section II. In Section III, we model user statistics per small cell and interferer statistics per apartment. We also formulate an expression of the optimal amount of spectrum per MNO for an arbitrary number of MNOs in a country. In Section IV, we derive average capacity, SE, EE, and Cost Efficiency (CE) metrics for the proposed, as well as the traditional Static Licensed Spectrum Allocation (SLSA), techniques. In addition, we show mathematically the outperformance of the proposed technique over the SLSA technique. In Section V, extensive numerical and simulation results and analyses for an example scenario of a country consisting of four MNOs are carried out by varying the effect of the spectrum reuse and the co-channel interference of interferer user equipments (UEs) within each apartment. Moreover, we also show that the proposed technique with two extreme CCI scenarios, including no CCI and the maximum CCI, for an MNO can achieve the SE and EE requirements for 6G mobile systems. Section VI covers the discussion on the offered benefits of the proposed technique, as well as its further research directions. We conclude the paper in Section VII. In Appendix A, a list of acronyms/abbreviations is shown in Table A1, and a list of selected notations is given in Table A2.

E. Declaration

This paper is an extended version of the work Saha [1] presented at The Fifteenth International Conference on Systems and Networks Communications (ICSNC), Porto, Portugal, 2020. The conference article Saha [1] has been extended in two major directions as follows.

- With introducing the 60 GHz unlicensed spectrum, and
- Without introducing the 60 GHz unlicensed spectrum,

in addition to the 28 GHz licensed spectrum to each small cell such as in [1].

Particularly, we have reported the extended journal version of [1] concerning the allocation and reuse of both the 28 GHz licensed spectrum and 60 GHz unlicensed spectrum in [22], whereas the allocation and reuse of only the 28 GHz licensed spectrum in this paper.

The conference article Saha [1] is used as the basis of both journal versions (i.e., [22] and this paper), which differ mainly from Saha [1] in terms of enhancement of background material, expansion of discussion, and inclusion of new problems and results. More specifically, in both journal versions, as compared to Saha [1],

- We model user statistics per small cell and interferer statistics per apartment in a building.
- We show mathematically the outperformance of the proposed technique over the traditional SLSA technique.
- We also clarify the simulation parameters and assumptions used for generating the performance results.
- A more detailed performance evaluation and analysis than that in Saha [1] are carried out by varying the effect of the spectrum reuse (both vertically within a building and horizontally in between buildings) and the co-channel interference (by considering all possible number of interferer UEs within each apartment).
- Finally, in addition to the offered benefits of the proposed technique, we discuss its future research directions.

Note that due to an extended version of Saha [1] and being [22] published earlier than this paper, some materials in this paper, in terms of, e.g., text, equations, figures, tables, notations, and abbreviations, may be found merged with that in [22] by citing [22]. Finally, this paper is written such that the readers will find it self-contained, detailed, and insightful in contrast to its conference version Saha [1].

II. System Architecture, Proposed Technique and Interference Management

A. System Architecture

Figure 1 shows the system architecture consisting of four MNOs, defined as MNO 1, MNO 2, MNO 3, and MNO 4, operating in a country. We assume that all MNOs have similar system architectural features including three types of Base Stations (BSs), namely macrocell BSs (MBSs), Picocell BSs (PBSs), and Small Cell BSs (SBSs). Hence, for simplicity in evaluating the performances, the detailed architecture of only one MNO, i.e., MNO 1, is shown in Figures 1(a) and 1(b). SBSs are deployed only within 3-dimensional multistory buildings (Figure 1(b)). Both SBSs and PBSs are located within the coverage of an MBS. All macrocell UEs per MBS are served either by the MBS itself or any PBSs. Due to the favorable characteristics, MBSs and PBSs operate at a low-frequency band, i.e., 2 GHz, whereas all in-building SBSs operate at the 28 GHz mmWave band (Figure 1(a)).

We consider that each MNO is given access to the countrywide 28 GHz mmWave spectrum to extend its spectrum at all times by enforcing the frequency-domain CCI management scheme, as shown in Figure 1(c). Given that CCI for an MNO o increases with an increase in the number of UEs of other MNOs $\boldsymbol{O}\backslash o$ (Figure 1(c) for MNO 1), Figure 1(c) shows all possible CCI scenarios for a small cell in an apartment of MNO 1 on a floor based on the presence of UEs of other MNOs $\boldsymbol{O}\backslash o$ within the same apartment of a building. For simplicity, CCI scenarios are shown for a single small cell each serving one UE at a time in an apartment on a floor. Besides, the penetration loss of a typical reinforced concrete floor in the 28 GHz mmWave spectrum is about 55 dB for the first floor [23][24][25]. Hence, by exploiting the high floor penetration loss of the 28 GHz mmWave spectrum, on top of the spectrum extension by allocating the countrywide massive 28 GHz spectrum to each MNO, we consider the spectrum exploitation by reusing the same countrywide spectrum to SBSs of each MNO on each floor of a building to increase spectral utilization (Figures 1(b) and 1(c)). We propose a technique for the spectrum allocation and the spectrum exploitation of the countrywide 28 GHz spectrum to each MNO in what follows.

B. Proposed Technique

We propose a countrywide mmWave spectrum allocation and reuse (CoMSAR) technique to extend the available spectrum for an MNO and to increase its utilization as follows.

Each MNO of a country is assigned with the massive 28 GHz mmWave spectrum specified countrywide, which is reused further, to operate its small cells deployed on each floor in a building at the cost of paying the spectrum licensing fee subject to avoiding CCI. The amount of the spectrum licensing fee for an MNO is updated corresponding to the change in its number of subscribers at each license renewal term t_{rnw}.

In this regard, for the 28 GHz mmWave spectrum allocation, each MNO is allocated to the countrywide 28 GHz mmWave spectrum by the National Regulatory Agency (NRA) or any third party for a term t_{rnw}. For the 28 GHz mmWave spectrum reuse, each MNO can exploit the high floor penetration loss of a multistory building at mmWave such that the allocated countrywide full 28 GHz mmWave spectrum can be reused to its SBSs deployed on each floor due to the insignificant or no CCI generated between adjacent floors (Figure 1(b)). This results in reusing the allocated countrywide spectrum to an MNO more than once to its SBSs within a multistory building and, hence, improving the countrywide 28 GHz mmWave spectrum utilization.

Each MNO pays the licensing fee to the NRA, which is defined by the administration based on the ratio of its actual number of subscribers to the sum of the total number of subscribers of all MNOs countrywide at t_{rnw}. Hence, the proposed technique can help overcome the lack of a sufficient amount of spectrum of an MNO to serve the necessary demand of its users, as well as address the issue of the under-utilized or unused spectrum of other MNOs, which in turn improve the overall countrywide spectrum utilization. Also, an MNO pays the licensing fee only for the amount of spectrum that it uses at any term t_{rnw} (i.e., in accordance with its number of users).

C. Co-channel Interference Management

Since all MNOs consider operating in-building small cells at the same countrywide 28 GHz mmWave spectrum, CCI occurs when small cell UEs of more than one MNO on the same floor in a building are scheduled to the same frequency simultaneously. Such CCI can be avoided by allocating UEs orthogonally in the frequency domain [26]. More specifically, UEs of MNOs located on the same floor in a building are allocated orthogonally to different parts of the countrywide 28 GHz mmWave spectrum, as shown in Figure 2. Hence, UEs of not more than one MNO can be allocated to the same frequency in any Transmission Time Interval (TTI). The existence of an interfering UE can be detected either by the small cell or the small cell UE itself using any conventional spectrum sensing techniques.

III. Mathematical Analysis

A. Modeling User Statistics per Small Cell

Like [22], we first model user statistics per small cell in this section. We are interested in finding the number of users per small cell of an MNO o in an apartment for an observation time Q. Let $U_s \in \boldsymbol{U}_s = \left\{0,1,2,...,U_{s,\max}\right\}$ denote the number of UEs served by an SBS s of an MNO o at any time t. According to [27][28], sessions or call arrivals can be modeled as a Poisson process. Hence, the traffic activity of a small cell UE served by an in-building SBS can be modeled as an exponentially distributed continuous-time Poisson process. Since given the present state, the future state is independent of the past state, the traffic activity of a UE can be modeled as a two-state Markov chain where the off-state traffic activity to on-state traffic activity transition rate of a UE is denoted by λ and the on-state traffic activity to off-state traffic activity transition rate is denoted by μ.

Let $p(0), p(1), p(2), \cdots, p(U_{s,\max})$ denote the on-state probabilities of an SBS s (corresponding to the number of active UEs U_s) in an apartment. The values of these probabilities can be found following the Birth-Death process [27] as shown in Figure 3. Let λ_{U_s} and μ_{U_s} denote, respectively, the birth rate and the death rate. Then, according to [29] [30], the followings hold.

$$\lambda_{U_s} = \begin{cases} \left(U_{s,\max} - U_s\right)\lambda, & 0 \le U_s \le U_{s,\max} \\ 0, & \text{otherwise} \end{cases}$$

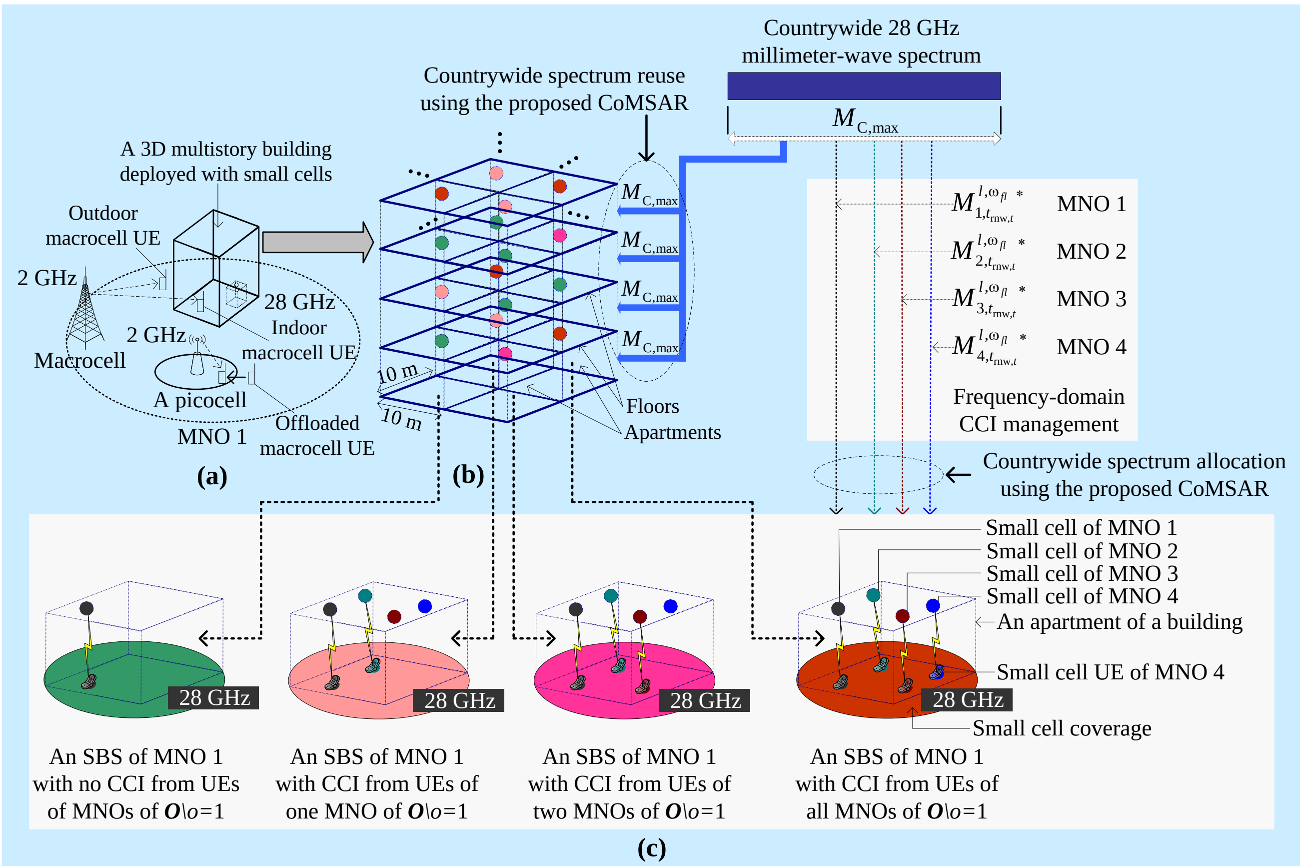

Figure 1. A system architecture consisting of four MNOs countrywide.

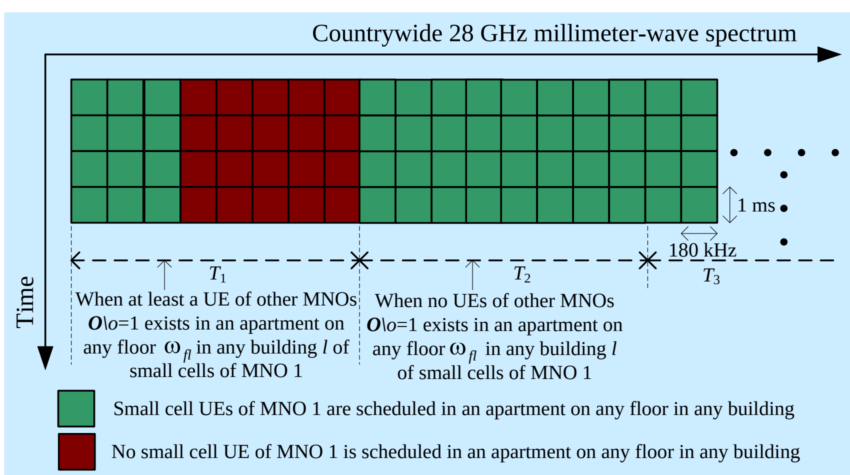

Figure 2. The frequency-domain CCI avoidance technique for UEs of MNO 1 in an apartment on any floor ω_{fl} in a building l. T_1, T_2, and T_3 define arbitrary and equal observation time intervals within $|\boldsymbol{T}| = Q$ [1].

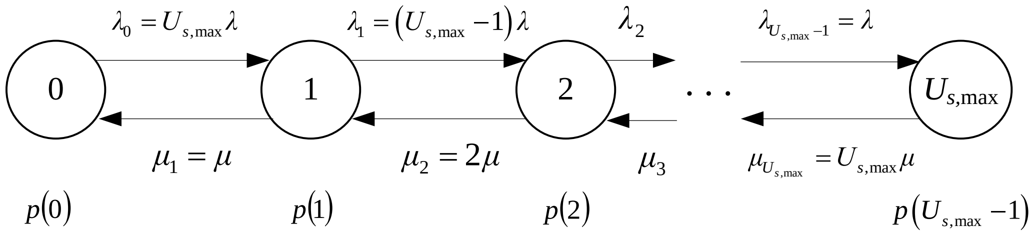

Figure 3. Occupancy or traffic in-progress state diagram for UEs per small cell in an apartment.

$\mu_{U_s} = U_s \times \mu$

Hence, the probability of any U_s can be given by,

$$p(U_s) = p(0)\left((\lambda/\mu)^{U_s} \times \binom{U_{s,\max}}{U_s}\right) \tag{1}$$

But, $\sum_{U_s=0}^{U_{s,\max}} p(U_s) = 1$ (2)

Then, using (1) and (2), the following can be obtained.

$$p(0) = 1/(1+(\lambda/\mu))^{U_{s,\max}}$$

Now from (1), we can find the following. In other words, the probability that U_s number of UEs are served by an SBS s is given by,

$$p(U_s) = \frac{U_{s,\max}!}{U_s!(U_{s,\max} - U_s)!} \times (\lambda/\mu)^{U_s} \times \frac{1}{(1+(\lambda/\mu))^{U_{s,\max}}} \tag{3}$$

Hence, the *expected value* of the number of UEs served simultaneously at any time t is then given by,

$$E[U_s] = \sum_{U_s=0}^{U_s=U_{s,\max}} (U_s \times p(U_s)) \tag{4}$$

Note that, since the rate of arrival of UEs to any in-building SBS s is relatively low due to the small coverage, the value of U_s is small in the *Poisson* distribution of small cell UEs [22]. In other words, smaller values of U_s are more probable than the larger ones such that the distribution of small cell UEs of an SBS lies mostly toward the left of the curve.

B. Optimal Amount of Spectrum per MNO

Let O denote the maximum number of MNOs of a country such that $o \in \boldsymbol{O} = \{1,2,...,O\}$. Let $S_{\mathrm{F},o}$ denote the total number of small cells of an MNO o in any building $l \in \boldsymbol{L} = \{1,2,3,...,L\}$ such that $s_{x,o} \in \boldsymbol{S}_{\boldsymbol{x,o}} = \{0,1,2,...,S_{\mathrm{F},o}\}$. Denote $M_{\mathrm{C,max}}$ as the countrywide total amount of mmWave spectrum defined in terms of the number of Resource Blocks (RBs) where an RB is equal to 180 kHz. Assume that $E[U_{s,o}] = 1$, i.e., each small cell $s_{x,o}$ of an MNO o can serve the maximum of one UE at a time.

Let $N_{o,t_{\mathrm{rnw}}}$ denote the total number of subscribers of an MNO o such that $\sum_{o}^{O} N_{o,t_{\mathrm{rnw}}} \le N_{\mathrm{C,\,max},t_{\mathrm{rnw}}}$ where $N_{\mathrm{C,\,max},t_{\mathrm{rnw}}}$ denotes the maximum number of subscribers of a country at term t_{rnw}. Also, UEs of not more than one MNO o on the same floor ω_{fl} can be served at the same RBs in any TTI in a building l. The amount of spectrum allocated to UEs of an MNO o on a floor ω_{fl} in a building l at term t_{rnw} in TTI t is defined as follows.

The amount of spectrum allocated to UEs of an MNO o on any floor ω_{fl} in a building l at term t_{rnw} is defined in accordance with the ratio of the number of subscribers $N_{o,t_{\mathrm{rnw}}}$ of the MNO o to the sum of the total number of subscribers $N_{t_{\mathrm{rnw}},t}^{l,\omega_{fl}}$ of all MNOs O corresponding to the same floor ω_{fl} in the building l in any TTI t at term t_{rnw}.

Note that the radio spectrum is not free of cost. Hence, licensing more spectrum causes an increase in the cost of an MNO. Moreover, as the total amount of the spectrum specified for a country is fixed, licensing more spectrum by one MNO causes the scarcity of the required spectrum by another MNO in a country, resulting in degrading the quality-of-service (QoS). This problem can be addressed if each MNO takes the license of the amount of the spectrum as low as possible corresponding to its actual number of subscribers so that the issue of the under-utilized or unused spectrum by one MNO, as well as the lack of a sufficient amount of spectrum for another MNO, to serve its necessary user demand can be addressed.

Since each MNO favors minimizing the cost of licensing spectrum while ensuring to serve its user demands adequately to retain QoS, we consider a minimization problem for allocating the countrywide mmWave spectrum to each MNO to increase the overall countrywide mmWave spectrum utilization. Hence, the optimal amount of licensed spectrum $M_{o,t_{\mathrm{rnw},t}}^{l,\omega_{fl}}$ in RBs for an MNO $o \in \boldsymbol{O}$ on any floor ω_{fl} in a building l in TTI t at a renewal term t_{rnw} can be found by solving the following problem.

$$\min_{o\in\boldsymbol{O}} \quad M_{o,t_{\text{rnw},t}}^{l,\omega_{fl}}$$
$$\text{subject to} \quad \text{(a) } N_{o,t_{\text{rnw}}} \Big/ N_{t_{\text{rnw}},t}^{l,\omega_{fl}} = M_{o,t_{\text{rnw},t}}^{l,\omega_{fl}} \Big/ M_{\text{C,max}} \qquad (5)$$
$$\text{(b) } \forall o \forall t_{\text{rnw}} \sum\nolimits_{o}^{O} N_{o,t_{\text{rnw}}} \le N_{\text{C, max},t_{\text{rnw}}}$$

The solution to the above optimization problem can be expressed as follows and is given in Proof 1.

$$M_{o,t_{\text{rnw},t}}^{l,\omega_{fl}\ *} = \left\lceil \left(\left(N_{o,t_{\text{rnw}}} \Big/ \sum_{o=1}^{O} \left(1_{\nu_o}\left(N_{o,t_{\text{rnw}}} \right) \times N_{o,t_{\text{rnw}}} \right) \right) \times M_{\text{C,max}} \right) \right\rceil \qquad (6)$$

Proof 1: The solution to the optimization problem in (5) can be found as follows. In general, the number of subscribers of all MNOs is not the same at any t_{rnw}. Hence, assume that $N_{1,t_{\text{rnw}}} > N_{2,t_{\text{rnw}}} > ... > N_{O,t_{\text{rnw}}}$ at t_{rnw} such that the constraint 5(b) is satisfied. Since a UE of any MNO $\boldsymbol{O}\backslash o$ in any TTI may not exist on any floor ω_{fl} in a building *l* of small cells of an MNO *o*, $N_{t_{\text{rnw}},t}^{l,\omega_{fl}}$ can be expressed for *O*=4 as

$$N_{t_{\text{rnw}},t}^{l,\omega_{fl}} = \sum_{o=1}^{O} \left(1_{\nu_o}\left(N_{o,t_{\text{rnw}}} \right) \times N_{o,t_{\text{rnw}}} \right) \qquad (7)$$

where $\nu_o \in \left\{ N_{1,t_{\text{rnw}}}, N_{2,t_{\text{rnw}}}, N_{3,t_{\text{rnw}}}, N_{4,t_{\text{rnw}}} \right\}$. $1(\cdot)$ defines that $1(\cdot)=1$ if $N_{o,t_{\text{rnw}}}$ exists in the set ν_o; otherwise, $1(\cdot)=0$.

Since the number of RBs is strictly an integer, using (7), and the constraint 5(a), the optimal value of $M_{o,t_{\text{rnw},t}}^{l,\omega_{fl}}$ is given by

$$M_{o,t_{\text{rnw},t}}^{l,\omega_{fl}\ *} = \left(N_{o,t_{\text{rnw}}} \Big/ N_{t_{\text{rnw}},t}^{l,\omega_{fl}} \right) \times M_{\text{C,max}}$$

$$M_{o,t_{\text{rnw},t}}^{l,\omega_{fl}\ *} = \left\lceil \left(\left(N_{o,t_{\text{rnw}}} \Big/ \sum_{o=1}^{O} \left(1_{\nu_o}\left(N_{o,t_{\text{rnw}}} \right) \times N_{o,t_{\text{rnw}}} \right) \right) \times M_{\text{C,max}} \right) \right\rceil \qquad \blacksquare$$

Note that if a UE of any MNO $\boldsymbol{O}\backslash o$ in any TTI *t* on any floor ω_{fl} in a building *l* does not exist, then $N_{t_{\text{rnw}},t}^{l,\omega_{fl}} = N_{o,t_{\text{rnw}}}$ in (7), which results in $M_{o,t_{\text{rnw},t}}^{l,\omega_{fl}\ *} = M_{\text{C,max}}$. This implies that the whole countrywide 28 GHz mmWave spectrum can be allocated in all TTIs *t* to UEs of small cells of an MNO *o* on any floor ω_{fl} in a building *l*. The same process described above is applicable for all MNOs $o \in \boldsymbol{O}$ at each renewal term t_{rnw} to update $M_{o,t_{\text{rnw},t}}^{l,\omega_{fl}\ *}$ in any TTI *t* to avoid CCI [22]. Hence, using (6), the countrywide 28 GHz spectrum can be reused to small cells of each MNO *o* on any floor ω_{fl} in a building *l* at the cost of paying the licensing fee based on $N_{o,t_{\text{rnw}}}$ of the corresponding MNO *o* at t_{rnw} with respect to that of other MNOs $\boldsymbol{O}\backslash o$ to improve countrywide 28 GHz mmWave spectrum utilization. Further, the higher the number of subscribers $N_{o,t_{\text{rnw}}}$ of an MNO *o* at term t_{rnw}, the greater the amount of mmWave spectrum $M_{o,t_{\text{rnw},t}}^{l,\omega_{fl}}$ allocated to MNO *o* on any floor ω_{fl} in a building *l* in any TTI *t* at term t_{rnw}.

C. Modeling Interferer Statistics per Apartment

Following [22], recall that we assume $E\left[U_{s,o}\right]=1$ for each SBS of each MNO *o* within each apartment of any building. Since the arrival of a UE to any SBS in an apartment can be modeled as a Poisson process, under the above assumption, the presence of the number of interferer UEs in each apartment can be expressed following the same procedure presented for modeling the user statistics per small cell in Section III(A). In doing so, let $U_k \in \boldsymbol{U_k} = \left\{0,1,2,...,U_{k,\max}\right\}$ denote the number of interferer UEs served by each SBS of MNOs $\boldsymbol{O}\backslash o$ in any TTI *t* for an SBS *s* of MNO *o*, where $U_{k,\max} = O-1$. Then, the probability of U_k number of interferer UEs for an SBS *s* of MNO *o* in an apartment is given by,

$$p\left(U_k\right) = \frac{U_{k,\max}!}{U_k!\left(U_{k,\max}-U_k\right)!} \times \left(\lambda/\mu\right)^{U_k} \times \frac{1}{\left(1+\left(\lambda/\mu\right)\right)^{U_{k,\max}}} \qquad (8)$$

Hence, the *expected value* of the number of interferer UEs served simultaneously at any time *t* in an apartment for an SBS *s* of MNO *o* is then given by,

$$E\left[U_k\right] = \sum\nolimits_{U_k=0}^{U_k=U_{k,\max}} \left(U_k \times p\left(U_k\right)\right) \qquad (9)$$

From (9), it can be found that the maximum amount of spectrum is allocated to an MNO *o* when no interferer UEs of MNOs $\boldsymbol{O}\backslash o$ exist within an apartment on any floor (i.e., $E\left[U_k\right]=0$). Likewise, the minimum amount of spectrum is allocated to an MNO *o* when each interferer UE of MNOs $\boldsymbol{O}\backslash o$ exist within each apartment on any floor, i.e., $E\left[U_k\right]=\left(U_{k,\max}-1\right)$ [22].

IV. Performance Metrics Estimation and Analysis

A. Performance Metrics

Let $S_{\text{M},o}$ denote the number of macrocells, and $S_{\text{P},o}$ denotes the number of picocells per macrocell of an MNO *o*. Also, let $\boldsymbol{T}$ denote the simulation run time with the maximum time of *Q* (in time steps each lasting 1 ms) such that $\boldsymbol{T}$= {1, 2, 3,…,*Q*}. Let P_{MC}, P_{PC}, and P_{SC} denote, respectively, the transmission power of a macrocell, a picocell, and a small cell of an MNO *o*. Using Shannon's capacity formula, a link throughput at RB=*i* in TTI=*t* for an MNO *o* at t_{rnw} in bps per Hz is given by [31][32]

$$\sigma_{t,i,o}^{t_{\text{rnw}}}\left(\rho_{t,i,o}^{t_{\text{rnw}}}\right) = \begin{cases} 0, & \rho_{t,i,o}^{t_{\text{rnw}}} < -10\,\text{dB} \\ \beta \log_2\left(1+10^{\left(\rho_{t,i,o}^{t_{\text{rnw}}}(\text{dB})/10\right)}\right), & -10\,\text{dB} \le \rho_{t,i,o}^{t_{\text{rnw}}} \le 22\,\text{dB} \\ 4.4, & \rho_{t,i,o}^{t_{\text{rnw}}} > 22\,\text{dB} \end{cases} \qquad (10)$$

where β denotes the implementation loss factor.

Let $M_{\mathrm{MBS},o}$ denote the spectrum in RBs of a macrocell for an MNO o. Then, the total capacity of all macrocell UEs for an MNO o at t_{rnw} can be expressed as

$$\sigma_{\mathrm{MBS},o}^{t_{\mathrm{rnw}}} = \sum_{t=1}^{Q} \sum_{i=1}^{M_{\mathrm{MBS},o}} \sigma_{t,i,o}^{t_{\mathrm{rnw}}} \left(\rho_{t,i,o}^{t_{\mathrm{rnw}}}\right) \tag{11}$$

where σ and ρ are responses over $M_{\mathrm{MBS},o}$ RBs of all macro UEs in $t \in \boldsymbol{T}$ for an MNO o at t_{rnw}. If all SBSs $s_{\omega_{fl},o}$ on any floor ω_{fl} in a building l of an MNO o serves simultaneously in all TTI $t \in \boldsymbol{T}$, then, the aggregate capacity served by an SBS, all SBSs per floor ω_{fl}, as well as all SBSs on all floors ω_{FL} in a building l, of an MNO o at a renewal term t_{rnw} are given respectively by

$$\sigma_{\mathrm{FD},o,l,s_{x,o}}^{t_{\mathrm{rnw}},\omega_{fl}} = \sum_{t\in\boldsymbol{T}} \sum_{i=1}^{M_{o,t_{\mathrm{rnw}},t}^{l,\omega_{fl}\,*}} \sigma_{t,i,o}^{t_{\mathrm{rnw}}} \left(\rho_{t,i,o}^{t_{\mathrm{rnw}}}\right) \tag{12}$$

$$\sigma_{\mathrm{FD},o,l,s_{\omega_{fl},o}}^{t_{\mathrm{rnw}},\omega_{fl}} = \sum_{s_{x,o}=1}^{S_{\omega_{fl},o}} \sigma_{\mathrm{FD},o,l,s_{x,o}}^{t_{\mathrm{rnw}},\omega_{fl}} \tag{13}$$

$$\sigma_{\mathrm{FD},o,l}^{t_{\mathrm{rnw}},\omega_{\mathrm{FL}}} = \sum_{\omega_{fl}=1}^{\omega_{\mathrm{FL}}} \sigma_{\mathrm{FD},o,l,s_{\omega_{fl},o}}^{t_{\mathrm{rnw}},\omega_{fl}} \tag{14}$$

Due to a short distance between a small cell UE and its SBS and a low transmission power of an SBS, we assume similar indoor signal propagation characteristics for all L buildings per macrocell for an MNO o at t_{rnw}. Then, by linear approximation, the system-level average aggregate capacity, SE, and EE for all MNOs O countrywide at t_{rnw} for l=L can be given by

$$\sigma_{\mathrm{FD,cap},O}^{\mathrm{sys},t_{\mathrm{rnw}}}(L) = \sum_{o=1}^{O} \left(\sigma_{\mathrm{MBS},o}^{t_{\mathrm{rnw}}} + \left(L \times \sigma_{\mathrm{FD},o,l}^{t_{\mathrm{rnw}},\omega_{\mathrm{FL}}}\right)\right) \tag{15}$$

Since $\left(L \times \sigma_{\mathrm{FD},o,l}^{t_{\mathrm{rnw}},\omega_{\mathrm{FL}}}\right) >> \sigma_{\mathrm{MBS},o}^{t_{\mathrm{rnw}}}$, roughly, (15) can be given by

$$\sigma_{\mathrm{FD,cap},O}^{\mathrm{sys},t_{\mathrm{rnw}}}(L) \cong \sum_{o=1}^{O} \left(L \times \sigma_{\mathrm{FD},o,l}^{t_{\mathrm{rnw}},\omega_{\mathrm{FL}}}\right) \tag{16}$$

$$\sigma_{\mathrm{FD,SE},O}^{\mathrm{sys},t_{\mathrm{rnw}}}(L) = \sigma_{\mathrm{FD,cap},O}^{\mathrm{sys},t_{\mathrm{rnw}}}(L) \Big/ \left(\left(M_{\mathrm{C,max}} + \sum_{o=1}^{O} M_{\mathrm{MBS},o}\right) \times Q\right) \tag{17}$$

$$\sigma_{\mathrm{FD,EE},O}^{\mathrm{sys},t_{\mathrm{rnw}}}(L) = \left(\sum_{o=1}^{O} \begin{pmatrix} \left(L \times S_{\mathrm{F},o} \times P_{\mathrm{SC}}\right) \\ + \left(S_{\mathrm{P},o} \times P_{\mathrm{PC}}\right) + \left(S_{\mathrm{M},o} \times P_{\mathrm{MC}}\right) \end{pmatrix}\right) \Big/ \left(\sigma_{\mathrm{FD,cap},O}^{\mathrm{sys},t_{\mathrm{rnw}}}(L) / Q\right) \tag{18}$$

where $S_{\mathrm{F},o} = \sum_{\omega_{fl}=1}^{\omega_{\mathrm{FL}}} s_{\omega_{fl},o}$ denotes the total number of SBSs in any building l for an MNO o.

However, in a traditional SLSA technique, a fair allocation of the licensed mmWave spectrum to each MNO in a country is assumed, i.e., each MNO is given license exclusively for an equal amount of the mmWave spectrum of M RBs such that for O=4, $M_{\mathrm{C,max}} = 4M$. Now, using (14)-(18), the system-level average capacity, SE, and EE for all MNOs O countrywide at t_{rnw} for l=L can be given by

$$\sigma_{\mathrm{SLSA,cap},O}^{\mathrm{sys},t_{\mathrm{rnw}}}(L) = \sum_{o=1}^{O} \left(\sigma_{\mathrm{MBS},o}^{t_{\mathrm{rnw}}} + \left(L \times \sum_{\omega_{fl}=1}^{\omega_{\mathrm{FL}}} \sum_{s_{x,o}=1}^{S_{\omega_{fl},o}} \sum_{t\in\boldsymbol{T}} \sum_{i=1}^{M} \sigma_{s_{x,o},t,i,o}^{t_{\mathrm{rnw}},\omega_{fl}} \left(\rho_{s_{x,o},t,i,o}^{t_{\mathrm{rnw}},\omega_{fl}}\right)\right)\right) \tag{19}$$

$$\sigma_{\mathrm{SLSA,cap},O}^{\mathrm{sys},t_{\mathrm{rnw}}}(L) \cong \sum_{o=1}^{O} \left(L \times \sum_{\omega_{fl}=1}^{\omega_{\mathrm{FL}}} \sum_{s_{x,o}=1}^{S_{\omega_{fl},o}} \sum_{t\in\boldsymbol{T}} \sum_{i=1}^{M} \sigma_{s_{x,o},t,i,o}^{t_{\mathrm{rnw}},\omega_{fl}} \left(\rho_{s_{x,o},t,i,o}^{t_{\mathrm{rnw}},\omega_{fl}}\right)\right) \tag{20}$$

$$\sigma_{\mathrm{SLSA,SE},O}^{\mathrm{sys},t_{\mathrm{rnw}}}(L) = \sigma_{\mathrm{SLSA,cap},O}^{\mathrm{sys},t_{\mathrm{rnw}}}(L) \Big/ \left(\left(M_{\mathrm{C,max}} + \sum_{o=1}^{O} M_{\mathrm{MBS},o}\right) \times Q\right) \tag{21}$$

$$\sigma_{\mathrm{SLSA,EE},O}^{\mathrm{sys},t_{\mathrm{rnw}}}(L) = \left(\sum_{o=1}^{O} \begin{pmatrix} \left(L \times S_{\mathrm{F},o} \times P_{\mathrm{SC}}\right) + \\ \left(S_{\mathrm{P},o} \times P_{\mathrm{PC}}\right) + \left(S_{\mathrm{M},o} \times P_{\mathrm{MC}}\right) \end{pmatrix}\right) \Big/ \left(\sigma_{\mathrm{SLSA,cap},O}^{\mathrm{sys},t_{\mathrm{rnw}}}(L) / Q\right) \tag{22}$$

Now, let ε_{C} denote the cost of the countrywide 28 GHz mmWave spectrum $M_{\mathrm{C,max}}$. Recall that an MNO o pays the spectrum licensing fee based on its number of subscribers $N_{o,t_{\mathrm{rnw}}}$ at t_{rnw} with respect to that of all MNOs $N_{\mathrm{C,max},t_{\mathrm{rnw}}}$. Assume that an MNO o pays the spectrum licensing fee of ε_o corresponding to $N_{o,t_{\mathrm{rnw}}}$ at t_{rnw} such that ε_o can be given by

$$\varepsilon_o = \left(N_{o,t_{\mathrm{rnw}}} / N_{\mathrm{C,max},t_{\mathrm{rnw}}}\right) \times \varepsilon_{\mathrm{C}} \tag{23}$$

Now, define Cost Efficiency (CE) as the cost required per unit achievable average capacity (i.e., per bps) such that the CE at term t_{rnw} can be expressed as follows for both techniques.

$$\varsigma_{\mathrm{FD,CE},O}^{\mathrm{sys},t_{\mathrm{rnw}}} = \varepsilon_{\mathrm{C}} \Big/ \sigma_{\mathrm{FD,cap},O}^{\mathrm{sys},t_{\mathrm{rnw}}}(L) \tag{24}$$

$$\varsigma_{\mathrm{SLSA,CE},O}^{\mathrm{sys},t_{\mathrm{rnw}}} = \varepsilon_{\mathrm{C}} \Big/ \sigma_{\mathrm{SLSA,cap},O}^{\mathrm{sys},t_{\mathrm{rnw}}}(L) \tag{25}$$

B. *Performance Improvement*

Hence, the factor representing an improvement in average capacity, SE, EE, and CE due to applying the proposed technique can be expressed respectively as follows.

$$\varsigma_{\mathrm{cap},O,\mathrm{IF}}^{\mathrm{sys},t_{\mathrm{rnw}}} = \sigma_{\mathrm{FD,cap},O}^{\mathrm{sys},t_{\mathrm{rnw}}}(L) \Big/ \sigma_{\mathrm{SLSA,cap},O}^{\mathrm{sys},t_{\mathrm{rnw}}}(L) \tag{26}$$

$$\varsigma_{\mathrm{SE},O,\mathrm{IF}}^{\mathrm{sys},t_{\mathrm{rnw}}} = \sigma_{\mathrm{FD,SE},O}^{\mathrm{sys},t_{\mathrm{rnw}}}(L) \Big/ \sigma_{\mathrm{SLSA,SE},O}^{\mathrm{sys},t_{\mathrm{rnw}}}(L) \tag{27}$$

$$\varsigma_{\mathrm{EE},O,\mathrm{IF}}^{\mathrm{sys},t_{\mathrm{rnw}}} = \sigma_{\mathrm{FD,EE},O}^{\mathrm{sys},t_{\mathrm{rnw}}}(L) \Big/ \sigma_{\mathrm{SLSA,EE},O}^{\mathrm{sys},t_{\mathrm{rnw}}}(L) \tag{28}$$

$$\varsigma_{\mathrm{CE},O,\mathrm{IF}}^{\mathrm{sys},t_{\mathrm{rnw}}} = \varsigma_{\mathrm{FD,CE},O}^{\mathrm{sys},t_{\mathrm{rnw}}} \Big/ \varsigma_{\mathrm{SLSA,CE},O}^{\mathrm{sys},t_{\mathrm{rnw}}} \tag{29}$$

In the following, we analyze the outperformance given by (26)-(29) of the proposed CoMSAR technique over the traditional SLSA technique in terms of average capacity, SE, EE, and CE [22]. In doing so, we consider the countrywide subscriber statistics of all MNOs on any floor ω_{fl} in a building l at a renewal term t_{rnw} in time t. Assume that the number of countrywide subscribers of MNO 1, MNO 2, MNO 3, and MNO 4 are, respectively, 10%, 20%, 30%, and 40% of the total number of subscribers in a country. Since the spectrum is allocated to any MNO o in proportionate to its number of subscribers, using (6), the allocated spectrum to MNO 1, MNO 2, MNO 3, and MNO 4, are given, respectively, by $M_{1,t_{\text{rnw}},t}^{l,\omega_{fl}} = \left(0.1 \times M_{\text{C,max}}\right)$, $M_{2,t_{\text{rnw}},t}^{l,\omega_{fl}} = \left(0.2 \times M_{\text{C,max}}\right)$, $M_{3,t_{\text{rnw}},t}^{l,\omega_{fl}} = \left(0.3 \times M_{\text{C,max}}\right)$, and $M_{4,t_{\text{rnw}},t}^{l,\omega_{fl}} = \left(0.4 \times M_{\text{C,max}}\right)$.

Hence, the total amount of the spectrum used to serve user demands of all MNOs when employing the proposed CoMSAR technique is given by,

$$M_{O,t_{\text{rnw}},t}^{l,\omega_{fl},\text{CoMSAR}} = \left(0.1 \times M_{\text{C,max}}\right) + \left(0.2 \times M_{\text{C,max}}\right) + \left(0.3 \times M_{\text{C,max}}\right) + \left(0.4 \times M_{\text{C,max}}\right)$$

$$M_{O,t_{\text{rnw}},t}^{l,\omega_{fl},\text{CoMSAR}} = M_{\text{C,max}} \tag{30}$$

On the other hand, when employing the traditional SLSA technique, each MNO o is allocated to an equal amount of spectrum of $\left(0.25 \times M_{\text{C,max}}\right)$. However, the number of subscribers of MNO 1, MNO 2, MNO 3, and MNO 4 are not the same such that each MNO does not need the same amount of spectrum. More specifically, since the amount of spectrum required to serve the user demand of any MNO varies in accordance with its number of subscribers, MNO 1, MNO 2, MNO 3, and MNO 4 can use, respectively, 10%, 20%, 25%, and 25% of $M_{\text{C,max}}$. Hence, the total amount of the spectrum used to serve user demands of all MNOs when employing the SLSA technique is given by,

$$M_{O,t_{\text{rnw}},t}^{l,\omega_{fl},\text{SLSA}} = \left(0.1 \times M_{\text{C,max}}\right) + \left(0.2 \times M_{\text{C,max}}\right) + \left(0.25 \times M_{\text{C,max}}\right) + \left(0.25 \times M_{\text{C,max}}\right)$$

$$M_{O,t_{\text{rnw}},t}^{l,\omega_{fl},\text{SLSA}} = 0.8 \times M_{\text{C,max}} \tag{31}$$

From (30) and (31), we can write the following.

$$M_{O,t_{\text{rnw}},t}^{l,\omega_{fl},\text{CoMSAR}} > M_{O,t_{\text{rnw}},t}^{l,\omega_{fl},\text{SLSA}} \tag{32}$$

Since the achievable capacity is directly proportional to the spectrum bandwidth, the following relation holds.

$$\sigma_{O,t_{\text{rnw}},t}^{l,\omega_{fl},\text{CoMSAR}} > \sigma_{O,t_{\text{rnw}},t}^{l,\omega_{fl},\text{SLSA}}$$

where $\sigma_{O,t_{\text{rnw}},t}^{l,\omega_{fl},\text{CoMSAR}} \propto M_{O,t_{\text{rnw}},t}^{l,\omega_{fl},\text{CoMSAR}}$ and $\sigma_{O,t_{\text{rnw}},t}^{l,\omega_{fl},\text{SLSA}} \propto M_{O,t_{\text{rnw}},t}^{l,\omega_{fl},\text{SLSA}}$ denote, respectively, the achievable capacities corresponding to the spectra in (30) and (31) due to employing the proposed CoMSAR and SLSA techniques.

Since SE is directly proportional, whereas EE and CE are inversely proportional, to the achievable capacity, using (17) and (21) for the SE, (18) and (22) for the EE, and (24) and (25) for the CE, it can be shown that the proposed CoMSAR technique provides better SE, EE, and CE performances than the traditional SLSA technique [22].

V. Performance Evaluation

A. Default Parameter and Assumption

Table I shows the default simulation parameters and assumptions used for evaluating the performance of the proposed technique for all MNOs O countrywide. The performance metrics are derived analytically for an arbitrary number of MNOs in a country and the evaluation is carried out for four MNOs (i.e., O=4) as an example scenario. The arrival of mobile traffic to a small cell is captured using the Poisson process to model the presence of UEs of MNOs within each apartment. Simulation assumptions and parameters used for the performance evaluation are in line with the recommendations from the standardization bodies such as the 3rd generation partnership project (3GPP) and International Telecommunication Union-Radiocommunication Sector (ITU-R).

For simplicity in analysis and finding a closed-form expression, we assume that each small cell of an MNO o can serve one UE at a time, i.e., $E\left[U_{s,o}\right] = 1$. Moreover, because of the favorable signal propagation characteristics in indoor environments and the availability of large spectrum bandwidth, we consider the 28 GHz millimeter-wave spectrum bands to serve high data rates within a short distance. However, all the macrocells and picocells are considered to operate at the 2 GHz band to provide large coverage and less number of hand-offs. Because high-frequency signals exhibit a low multi-path fading effect indoors, the Line-Of-Sight (LOS) large-scale signal propagation model is assumed for 28 GHz. Further, due to serving a UE at a short distance over a LOS channel by an SBS, similar signal propagation characteristics are considered within the same building, as well as between adjacent buildings.

Because of a high external wall penetration loss, low transmission power, and the existence of distance-dependent path loss for the distance in-between adjacent buildings for high-frequency signals, we assume an insignificant CCI effect from SBSs of one building to that of adjacent buildings resulting in reusing the same spectrum to SBSs within each building. Furthermore, we adopt the full buffer traffic model to consider serving user traffic at all times and the proportional fair scheduler to provide a balanced trade-off between the fairness and throughput performances. The performance results are generated by a simulator built using the computational tool MATLAB R2012b taking into account all parameters and assumptions stated above and given in Table I. Finally, the algorithm used to generate the performance results is given in Algorithm 1.

B. Performance Result and Analysis

The performance of the proposed technique is evaluated with regard to the traditional SLSA technique. We assume that MNO 1, MNO 2, MNO 3, and MNO 4 have the number of subscribers of 40%, 30%, 20%, and 10%, respectively, of the total number of subscribers countrywide $N_{C,\max,t_{\rm rnw}}$ at any term $t_{\rm rnw}$ (Table I).

1) Impact of the CCI

The performance of the proposed technique is evaluated for UEs of MNO 1 by varying the number of co-channel interferer UEs of I_{CCI}=0 to I_{CCI}=3 of MNOs $\boldsymbol{O}\backslash o$=1 per apartment on a single floor of a building for a country with O=4 MNOs. Figure 4 shows the performance improvement of the proposed technique in terms of the average capacity, SE, EE, and CE with respect to that of the traditional SLSA technique. Note that we consider the worst-case scenario, i.e., $M_{1,t_{\rm rnw},t}^{l,\omega_{fl}\ *}$ is minimum in (6), such that I_{CCI}=1 corresponds to a UE of MNO=2 with 30% of subscribers, and I_{CCI}=2 corresponds to UEs of MNO=2 and MNO=3 with 20% of subscribers. Whereas, I_{CCI}=0 and I_{CCI}=3 correspond to two extreme scenarios, including when no CCI occurs due to the absence of UEs of all other MNOs $\boldsymbol{O}\backslash o$=1, and when the maximum CCI occurs due to the presence of UEs of each MNO of $\boldsymbol{O}\backslash o$=1 on a floor in a building.

With no co-channel interferer UEs in any apartment (i.e., I_{CCI}=0), the maximum amount of full countrywide mmWave spectrum can be allocated to SBSs of MNO 1 on each floor in all TTIs. As I_{CCI} increases, the amount of allocated spectrum to MNO 1 decreases, and for the maximum co-channel interferer UEs, I_{CCI}=3, only 40% of the countrywide spectrum can be allocated to SBSs of MNO 1 on each floor. Hence, the spectrum allocated to SBSs of MNO 1 on each floor with I_{CCI}=0 is 2.5 times $(1/0.4)$ of the allocated spectrum I_{CCI}=3.

Since the achievable capacity depends directly on the amount of spectrum, the maximum and minimum average capacity, SE, EE, and CE for MNO 1 can be achieved, respectively, with I_{CCI}=0 and I_{CCI}=3 as shown in Figure 4. Moreover, Figure 4 also shows that the proposed technique with no CCI provides 2.5 times higher average capacity, SE, EE, and CE performances than that with the maximum CCI. Furthermore, with regard to the traditional SLSA, the proposed technique improves the average capacity, SE, EE, and CE of MNO 1 by 300%, 165%, 75%, and 60%, respectively with no co-channel interferer UEs, I_{CCI}=0. The improvement factors, however, decrease as I_{CCI} increases and get to a minimum when I_{CCI}=3. Hence, CCI plays a vital role in the overall performance of an MNO when allocated to the countrywide spectrum.

2) Effect of the Spectrum Reuse

Figures 5(a) and 5(b) show the effect of reusing the same countrywide spectrum both vertically to each floor of SBSs of MNO 1 in a multistory building and horizontally to each building over a macrocell coverage. As can be seen from Figure 5, the proposed technique provides better SE and EE performances than the traditional SLSA technique, with the variation of either ω_{FL}, or L, or both. Moreover, with an increase in the number of floors ω_{FL}, i.e., vertical reuse factor (RF), as well as the number of buildings L, i.e., horizontal RF, SE increases linearly, whereas EE increases negative exponentially, irrespective of the degree of CCI. Note, however, that since SE is affected additionally by the optimal amount of countrywide spectrum, the proposed technique with the maximum CCI provides insignificant SE while noticeable EE improvement over the traditional SLSA technique because of its higher average capacity performance, as shown in Figures 5(a) and 5(b).

Hence, the performance of the proposed technique is greatly influenced by the CCI, and a significant performance gain can be achieved when the aggregate CCI is limited to a low value. However, due to a small coverage of an indoor small cell and a low probability of co-existing all interferer UEs of MNOs $\boldsymbol{O}\backslash o$=1 within an apartment, the proposed technique can improve considerably the average SE and EE performances. Moreover, the impact of CCI can be compensated by increasing the RF. For example, the proposed technique with the maximum CCI for vertical RF=6 or more can provide better SE and EE performances than when operating under no CCI scenarios for vertical RF=1 for any horizontal RF.

C. Performance Comparison

According to [39][40], the future 6G mobile systems are expected to require 10 times average SE (i.e., 270-370 bps/Hz), as well as 10 times average EE (i.e., 0.3×10^{-6} Joules/bit), of that of 5G mobile systems [41][42]. Using Figure 5, Table II shows the variation in the required values of the vertical RF ω_{FL} and horizontal RF L when employing the traditional SLSA technique and the proposed technique with no CCI, as well as the maximum CCI, scenarios for each apartment on each floor of any building for MNO 1 to satisfy both the SE and EE requirements for 6G mobile systems.

From Table II, it can be found that the required SE and EE for 6G can be achieved by changing either vertical RF ω_{FL} or horizontal RF L such that their product, i.e., ($\omega_{FL}\times L$), defines the achievable SE and EE performances. Moreover, the proposed CoMSAR technique can satisfy both the SE of 370 bps/Hz and EE of 0.3 µJ/bit for 6G mobile systems by reusing (horizontally) the countrywide 28 GHz mmWave spectrum to small cells of MNO 1 of about 61.2% less number of single-floor (i.e., ω_{FL} =1) buildings (i.e., L=12) with no CCI, whereas 6.4% less number of single-floor buildings (i.e., L=29) with the maximum CCI, than that required by the traditional SLSA technique (i.e., L =31).

VI. OFFERED BENEFITS AND FURTHER OUTLOOKS

A. Offered Benefits

The proposed technique benefits from a number of issues as follows. Unlike the traditional SLSA technique, the proposed technique ensures the availability of a large amount of spectrum by allocating the countrywide full (instead of a portion) mmWave spectrum to each MNO. Further, it provides an efficient spectrum utilization by allowing each MNO dynamic and flexible (instead of static and dedicated) access to the countrywide spectrum [22]. Furthermore, it allows an MNO to pay only for the amount of spectrum that it uses to serve its user demands (i.e., in proportionate with the number of its users) at any term $t_{\rm rnw}$, resulting in reducing the cost per unit capacity (i.e., bps).

TABLE I. DEFAULT PARAMETERS AND ASSUMPTIONS

Parameters and Assumptions	Value	
28 GHz spectrum countrywide	200 MHz	
Number of MNOs and subscribers	4 and $N_{\mathrm{C,max}}$	
Number of subscribers for MNOs 1, 2, 3, and 4, respectively	40%, 30%, 20%, and 10% of $N_{\mathrm{C,max}}$	
For each MNO		
E-UTRA simulation case[1,6]	3GPP case 3	
Cellular layout[2,6], Inter-Site Distance (ISD)[1,2,6], transmit direction	Hexagonal grid, dense urban, 3 sectors per macrocell site, 1732 m, downlink	
Carrier frequency[2,5,6]	2 GHz Non-Line-Of-Sight (NLOS) for macrocells and picocells, 28 GHz LOS for all small cells	
Number of cells	1 macrocell, 2 picocells, 280 small cells per building	
Total BS transmit power[1] (dBm)	46 for macrocell[1,4], 37 for picocells[1], 19 for small cells[1,3,4]	
Co-channel small-scale fading model[1,3,5]	Frequency selective Rayleigh for 2 GHz, none for 28 GHz	
Path loss – MBS and a UE[1] – Outdoor macrocell UE	PL(dB)=15.3 + 37.6 $\log_{10}R$, R is in m	
Path loss – MBS and a UE[1] – Indoor macrocell UE	PL(dB)=15.3 + 37.6 $\log_{10}R + L_{\mathrm{ow}}$, R is in m	
Path loss – PBS and a UE[1]	PL(dB)=140.7+36.7 $\log_{10}R$, R is in km	
Path loss – SBS and a UE[1,2,5]	$PL(\mathrm{dB}) = 61.38 + 17.97\log_{10}(d)$, d is in m	
Lognormal shadowing standard deviation (dB)	8 for MBS[2], 10 for PBS[1], and 9.9 for SBS[2,5]	
Antenna configuration	Single-input single-output for all BSs and UEs	
Antenna pattern (horizontal)	Directional (120^0) for MBS[1], omnidirectional for PBS[1] and SBS[1]	
Antenna gain plus connector loss (dBi)	14 for MBS[2], 5 for PBS[1], 5 for SBS[1,3]	
UE antenna gain[2,3]	0 dBi (for 2 GHz), 5 dBi (for 28 GHz, Biconical horn)	
UE noise figure[2,3] and UE speed[1]	9 dB (for 2 GHz) and 10 dB (for 28 GHz), 3 km/hr	
Picocell coverage, number of macrocell UEs, and macrocell UEs offloaded to all picocells[1]	40 m (radius), 30, 2/15	
Indoor macrocell UEs[1]	35%	
3D multistory building and SBS models (square-grid apartments)	Number of buildings	L
	Number of floors per building	35
	Number of apartments per floor	8
	Number of SBSs per apartment	1
	Number of SBSs per building	280
	Area of an apartment	10×10 m^2
	Materials used	Reinforced concrete
Scheduler and traffic model[2]	Proportional Fair and full buffer	
Type of SBSs	Closed Subscriber Group femtocell BSs	
Channel State Information	Ideal	
TTI[1] and scheduler time constant (t_c)	1 ms and 100 ms	
Total simulation run time	8 ms	

taken [1]from [33], [2]from [34], [3]from [35], [4]from [36], from [5][37], from [6][38].

Algorithm 1. Proposed CoMSAR technique

Input: O=4, Q, t_{rnw}, $N_{\mathrm{C,\,max},t_{\mathrm{rnw}}}$ M, $N_{o,t_{\mathrm{rnw}}}$, $M_{\mathrm{C,max}}$, $S_{\mathrm{F},o}$, P_{MC}, P_{PC}, P_{SC}, $L_{\max}$, ω_{FL}

For $L = \{1, 2, 3, ..., L_{\max}\}$

  For t={1, 2, 3,…,Q}

    For $o \in \boldsymbol{O} = \{1, 2, ..., O\}$

      Find $M_{o,t_{\mathrm{mw},t}}^{l,\omega_{fl}\ *}$ using (6)

      Estimate Capacity, $\sigma_{\mathrm{FD,cap},O}^{\mathrm{sys},t_{\mathrm{mw}}}(L)$ and $\sigma_{\mathrm{SLSA,cap},O}^{\mathrm{sys},t_{\mathrm{mw}}}(L)$

      Estimate SE $\sigma_{\mathrm{FD,SE},O}^{\mathrm{sys},t_{\mathrm{mw}}}(L)$ and $\sigma_{\mathrm{SLSA,SE},O}^{\mathrm{sys},t_{\mathrm{mw}}}(L)$

      Estimate EE $\sigma_{\mathrm{FD,EE},O}^{\mathrm{sys},t_{\mathrm{mw}}}(L)$ and $\sigma_{\mathrm{SLSA,EE},O}^{\mathrm{sys},t_{\mathrm{mw}}}(L)$

      Estimate CE $\varsigma_{\mathrm{FD,CE},O}^{\mathrm{sys},t_{\mathrm{mw}}}$ and $\varsigma_{\mathrm{SLSA,CE},O}^{\mathrm{sys},t_{\mathrm{mw}}}$

    End

  End

End

Find improvement factors: $\varsigma^{\mathrm{sys},t_{\mathrm{mw}}}_{\mathrm{cap},O,\mathrm{IF}}$, $\varsigma^{\mathrm{sys},t_{\mathrm{mw}}}_{\mathrm{SE},O,\mathrm{IF}}$, $\varsigma^{\mathrm{sys},t_{\mathrm{mw}}}_{\mathrm{EE},O,\mathrm{IF}}$, $\varsigma^{\mathrm{sys},t_{\mathrm{mw}}}_{\mathrm{CE},O,\mathrm{IF}}$

Output: Display for MNO o=1: $\varsigma^{\mathrm{sys},t_{\mathrm{mw}}}_{\mathrm{cap},O,\mathrm{IF}}$ $\varsigma^{\mathrm{sys},t_{\mathrm{mw}}}_{\mathrm{SE},O,\mathrm{IF}}$ $\varsigma^{\mathrm{sys},t_{\mathrm{mw}}}_{\mathrm{EE},O,\mathrm{IF}}$, $\varsigma^{\mathrm{sys},t_{\mathrm{mw}}}_{\mathrm{CE},O,\mathrm{IF}}$

Plot: For no CCI and maximum CCI for MNO o=1: $\sigma^{\mathrm{sys},t_{\mathrm{mw}}}_{\mathrm{FD,SE},O}(L)$, $\sigma^{\mathrm{sys},t_{\mathrm{mw}}}_{\mathrm{SLSA,SE},O}(L)$, $\sigma^{\mathrm{sys},t_{\mathrm{mw}}}_{\mathrm{FD,EE},O}(L)$, $\sigma^{\mathrm{sys},t_{\mathrm{mw}}}_{\mathrm{SLSA,EE},O}(L)$

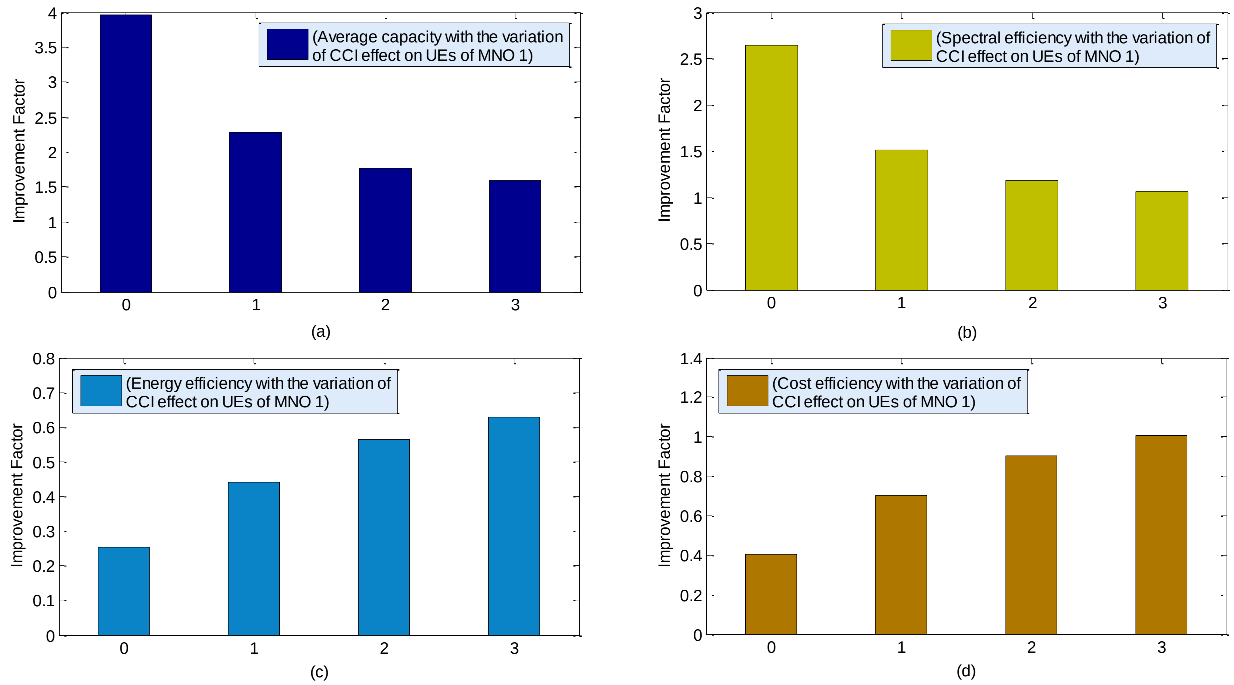

Figure 4. Performance improvement of the proposed CoMSAR technique with respect to that of the traditional SLSA technique due to the change in the number of co-channel interferer UEs of MNOs $\boldsymbol{O}\backslash o$=1 per apartment on a single floor of a building for UEs of MNO 1 of a country with O=4 MNOs. (a) average capacity, (b) spectral efficiency, (c) energy efficiency, and (d) cost efficiency.

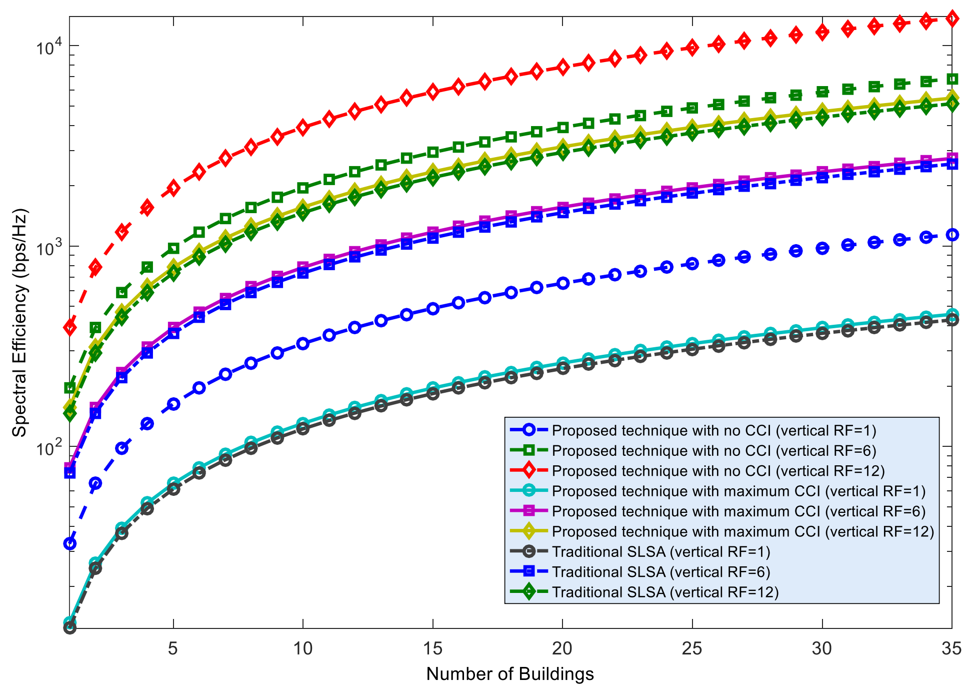

(a)

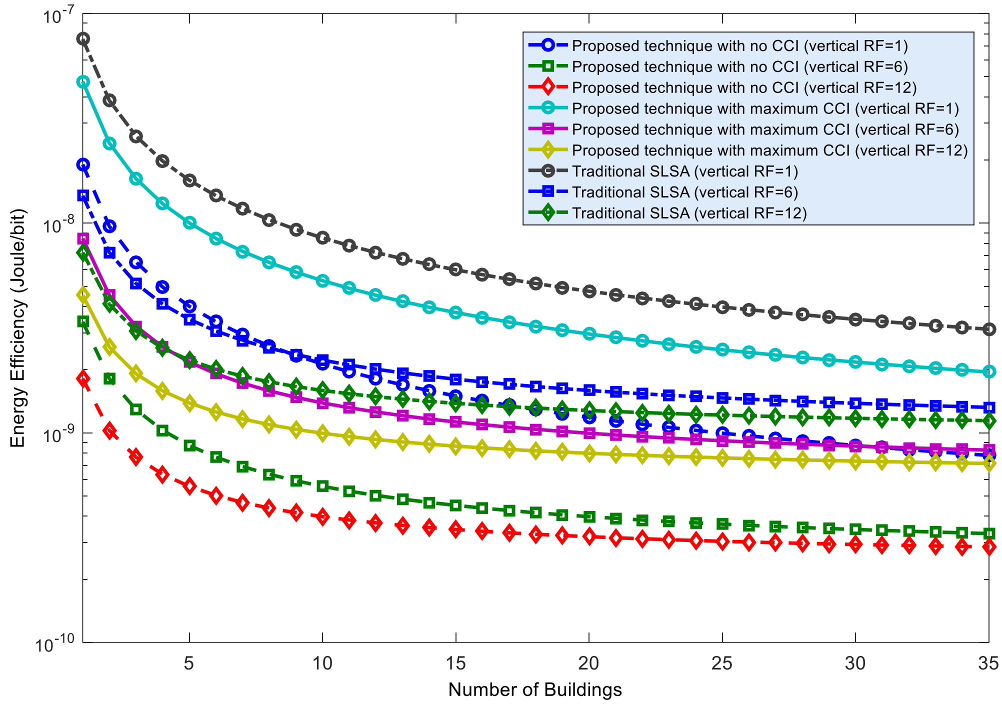

(b)

Figure 5. (a) SE and (b) EE performances of CoMSAR versus SLSA with a change in vertical RF and horizontal RF for MNO 1.

TABLE II. REQUIRED VERTICAL RF AND HORIZONTAL RF FOR THE PROPOSED AND SLSA TECHNIQUES TO SATISFY SE AND EE REQUIREMENTS FOR 6G MOBILE SYSTEMS.

Vertical RF	**Horizontal RF**								
	Proposed technique with no CCI		Proposed technique with maximum CCI		Traditional SLSA		Proposed technique with no CCI	Proposed technique with maximum CCI	Traditional SLSA
	SE	EE	SE	EE	SE	EE	Minimum required to satisfy SE and EE		
1	12	1	29	1	31	1	12	29	31
6	2	1	5	1	6	1	2	5	6
12	1	1	3	1	3	1	1	3	3

B. Further Outlooks

1) Implementation perspectives: The implementation of the proposed technique warrants the following issues [22], including updating the dynamic usage of the countrywide spectrum on each floor by UEs of different MNOs and enforcing CCI management. In this regard, SBSs of each MNO per floor can keep sensing using either a reactive or proactive approach to detect the status of the shared full countrywide spectrum usage and coordinate with SBSs of other MNOs on the same floor to update the CCI status and amount of the shared spectrum usage for each MNO. However, such coordination among SBSs of different MNOs generates a huge amount of control signaling overheads depending on the size of the group of the coordinated SBSs. The larger the size of the group of the coordinated SBSs, the greater the amount of generated control signaling overheads, as well as the delay in updating the CCI status.

In general, coordination among SBSs can be done centrally or in a distributed manner [22]. Central coordination of SBSs per building, for example, can contribute to achieving a global optimization in updating the CCI status and the corresponding spectrum allocation to each MNO. This, however, comes at the cost of generating high control signaling overheads. On the other hand, by limiting the size of a coordinated group of SBSs, control signaling overheads due to the coordination can be kept limited. This, however, comes at the cost of allowing a local optimization in updating the CCI status and the corresponding allocated spectrum to each MNO. Hence, a tradeoff between the optimal performance in the CCI and scheduled spectrum status updates per MNO and the generated control signaling overhead due to the coordination needs to be achieved, which asks for further studies [22]. We consider this issue as part of our future research studies.

2) Modeling 3D spectrum reuse: In this paper, we limit reusing the same countrywide full spectrum in small cells of an MNO *o* on each floor (i.e., 2-dimensional space) of a multistory building like [22]. However, the countrywide full spectrum allocated to an MNO o in the primary level can be exploited in the 3D space of a multistory building of small cells to increase the vertical RF even further for a building. More specifically, by enforcing a maximum CCI, a minimum distance between co-channel small cells (each located in an apartment) can be defined in both the intra-floor and inter-floor levels to form a 3D cluster of small cells of an MNO *o* within a building. The allocated spectrum per MNO can then be reused for each 3D cluster of small cells of an MNO *o* to improve the spectrum utilization. for example, adopting [13], a minimum distance between co-channel small cells for the 28 GHz mmWave spectrum in the intra-floor level and inter-floor level, respectively, for any MNO o at any term t_{rnw} can be expressed as follows [22].

$$\Delta_{\mathrm{a}} = \Delta_{\mathrm{m}} \times \left(\Xi_{\mathrm{a}} \big/ I_{\mathrm{a}}^{\mathrm{thr}} \right)^{(1/1.797)} \tag{33}$$

$$\Delta_{\mathrm{e}} \geq \Delta_{\mathrm{m}} \times \left(\left(\Xi_{\mathrm{e}} \big/ I_{\mathrm{e}}^{\mathrm{thr}} \right) \Big/ 10^{\left(\alpha_{\mathrm{f}}(\Delta_{\mathrm{e}})/10 \right)} \right)^{(1/1.797)} \tag{34}$$

where $I_{\mathrm{a}}^{\mathrm{thr}}$ and $I_{\mathrm{e}}^{\mathrm{thr}}$ denote, respectively, intra-floor and inter-floor CCI constraints at a small cell UE. Ξ_{a} and Ξ_{e} denote, respectively, the maximum number of co-channel small cells in the intra-floor level and inter-floor level. Δ_{m} denotes the minimum distance between a co-channel small cell and a small cell UE and $\alpha_{\mathrm{f}}(\Delta_{\mathrm{e}})$ denotes the floor penetration loss at 28 GHz.

Let s_l^{a} and s_l^{e} denote, respectively, the number of small cells corresponding to $\Delta_{\mathrm{a},l}$ and $\Delta_{\mathrm{e},l}$ in a building *l* such that a 3D cluster consists of $S_{\mathrm{3D},l} = \left(s_l^{\mathrm{a}} \times s_l^{\mathrm{e}} \right)$ small cells. Hence, the same spectrum of MNO *o* can be reused for each cluster of $\left(s_l^{\mathrm{a}} \times s_l^{\mathrm{e}} \right)$ small cells in a building. Let $S_{\mathrm{F},l}$ denote the maximum number of small cells of an MNO *o* in a building *l* such that the number of times the same spectrum of MNO *o* can be reused in building *l* (i.e., the spectrum RF for MNO *o* in building *l*) can be expressed as follows.

$$\omega_{\mathrm{3D},l} = \frac{S_{\mathrm{F},l}}{\left(s_l^{\mathrm{a}} \times s_l^{\mathrm{e}} \right)} \tag{35}$$

$$\omega_{\mathrm{3D},l} = \frac{S_{\mathrm{F},l}}{S_{\mathrm{3D},l}} \tag{36}$$

Since the spectrum reuse can be performed to small cells deployed on the same floor of a building and the 28 GHz mmWave signal faces high floor penetration loss, $\omega_{\mathrm{3D},l} \geq \omega_{\mathrm{FL},l}$ may satisfy, resulting in improving the average capacity, SE, EE, and CE even further. Like [22], we consider this issue as w part of our future studies.

3) Impact of frequency bands on spectrum exploitation: The distance-dependent path loss varies with a change in carrier frequency. In general, an increase in carrier frequency causes to increase the path loss. Since the usable mmWave frequencies range largely, there is a corresponding impact on the reuse of the mmWave spectrum. For example, the distance-dependent path loss for the 60 GHz mmWave band can be expressed as [43] $PL(dB) = 68 + 21.7\log_{10}(d)$ where *d* is in the meter [22]. Like the 28 GHz band, adopting [13], a minimum distance between co-channel small cells for the path loss of 60 GHz mmWave spectrum as given above in the intra-floor level and inter-floor level, respectively, for any MNO o can be expressed as follows [22].

$$\Delta_{\mathrm{a,60\,GHz}} = \Delta_{\mathrm{m}} \times \left(\Xi_{\mathrm{a}} \big/ I_{\mathrm{a}}^{\mathrm{thr}} \right)^{(1/2.17)} \tag{37}$$

$$\Delta_{\mathrm{e,60\,GHz}} \geq \Delta_{\mathrm{m}} \times \left(\left(\Xi_{\mathrm{e}} \big/ I_{\mathrm{e}}^{\mathrm{thr}} \right) \Big/ 10^{\left(\alpha_{\mathrm{f}}(\Delta_{\mathrm{e,60GHz}})/10 \right)} \right)^{(1/2.17)} \tag{38}$$

where Δ_{m}, Ξ_{a} and $I_{\mathrm{a}}^{\mathrm{thr}}$ for the intra-floor level, as well as Ξ_{e} and $I_{\mathrm{e}}^{\mathrm{thr}}$ for the inter-floor level, are the same for both the 28-GHz and 60-GHz mmWave bands. Now, taking the ratio of (37) to (33), we can find the following for the intra-floor level.

$$\frac{\Delta_{\mathrm{a,60\,GHz}}}{\Delta_{\mathrm{a,28\,GHz}}} = \left(\Xi_{\mathrm{a}} \big/ I_{\mathrm{a}}^{\mathrm{thr}} \right)^{(1/2.17)-(1/1.797)}$$

$$\frac{\Delta_{\mathrm{a,60\,GHz}}}{\Delta_{\mathrm{a,28\,GHz}}} = \left(\Xi_{\mathrm{a}} \big/ I_{\mathrm{a}}^{\mathrm{thr}} \right)^{-0.373}$$

However, $0 \leq I_{\mathrm{a}}^{\mathrm{thr}} \leq 1$ and Ξ_{a} is a positive integer such that the following holds.

$$\left(\Xi_{\mathrm{a}} \big/ I_{\mathrm{a}}^{\mathrm{thr}} \right)^{-0.373} < 1$$

Hence, $\Delta_{\mathrm{a,60\,GHz}} < \Delta_{\mathrm{a,28\,GHz}}$ (39)

This implies that the minimum distance in the intra-floor level decreases with an increase in frequency. Moreover, due to the higher frequency band, $\alpha_{\mathrm{f}}\left(\Delta_{\mathrm{e,60GHz}}\right) \geq \alpha_{\mathrm{f}}\left(\Delta_{\mathrm{e,28GHz}}\right)$. Hence, following the above procedure for the intra-floor level, it can be shown that the following holds for the inter-floor level.

$$\Delta_{\mathrm{e,60\,GHz}} < \Delta_{\mathrm{e,28\,GHz}} \tag{40}$$

Let $s_{l,\mathrm{60\,GHz}}^{\mathrm{a}}$ corresponds to $\Delta_{\mathrm{a,60\,GHz}}$ and $s_{l,\mathrm{60\,GHz}}^{\mathrm{e}}$ corresponds to $\Delta_{\mathrm{e,60\,GHz}}$ such that a 3D cluster at the 60 GHz band consists of $s_{\mathrm{3D},l,\mathrm{60\,GHz}} = \left(s_{l,\mathrm{60\,GHz}}^{\mathrm{a}} \times s_{l,\mathrm{60\,GHz}}^{\mathrm{e}} \right)$ small cells. Then, from (39) and (40), we can find the following.

$$\left(s_{l,60\text{GHz}}^{\text{a}} \times s_{l,60\text{GHz}}^{\text{e}}\right) < \left(s_{l,28\text{GHz}}^{\text{a}} \times s_{l,28\text{GHz}}^{\text{e}}\right)$$

$$s_{3\text{D},l,60\text{GHz}} < s_{3\text{D},l,28\text{GHz}} \quad (41)$$

Hence, the 3D cluster size decreases with an increase in frequency, i.e., more reuse of the same amount of spectrum bandwidth at the 60 GHz band can be made than that of the 28 GHz band for the same number of apartments in a building. Since there are other mmWave bands considered effective for the 5G and beyond mobile systems, including 26 GHz, 39 GHz, and 73 GHz, a detailed understanding of how the mmWave frequency bands impact their reuse in in-building scenarios is necessary [22], which we consider addressing as further studies.

4) MmWave spectrum allocation and reuse in outdoor environments: In this paper, we limit investigating the proposed countrywide mmWave spectrum allocation and reuse technique to indoor SBSs deployed in multistory buildings. However, the propagation characteristics of mmWave signals in outdoor environments differ greatly from those in indoor ones, particularly, rain and atmospheric absorption effect, cell coverage, shadowing effect from large buildings, outage probability, user density, and speed, and mobility and handover management. All these aspects have a significant impact on the allocation and reuse of the mmWave spectrum outdoors. Hence, how to allocate the countrywide mmWave spectrum to each MNO in outdoor environments without causing CCI to each other and reuse the same mmWave spectrum for any MNO spatially need considerable research work [22]. We aim to address this issue of the mmWave spectrum allocation and reuse in outdoor environments in our future research studies.

5) Effect of highly reflective environments: In general, the presence of LOS components is higher and the effect of multi-path fading from reflections, refractions, and scattering is less in high-frequency mmWave than in low-frequency microwave signals. So, even though, for simplicity, we consider no effect of highly reflective environments such as furniture and metal walls, ventilation installations, and elevator cars in the performance analysis of indoors in this paper, in practice, there may be some effects from such highly reflective environments in high-frequency signals. This requires further investigations, which we consider for our future studies.

VII. CONCLUSION

In this paper, we have proposed a countrywide millimeter-wave (mmWave) spectrum allocation and reuse (CoMSAR) technique that considers assigning each MNO with the 28 GHz mmWave spectrum countrywide at the cost of paying the spectrum licensing fee subject to avoiding co-channel interference (CCI). The assigned spectrum to each MNO is reused further to operate its small cells deployed on each floor in a multistory building. The amount of the spectrum licensing fee for an MNO is updated in accordance with its number of subscribers at each license renewal term. Moreover, CCI has been avoided by developing a frequency-domain CCI avoidance scheme that allocates UEs of different MNOs in an apartment on any floor of a building orthogonally to the countrywide 28 GHz mmWave spectrum. We have modeled user statistics per small cell and interferer statistics per apartment and formulated an expression for the optimal amount of spectrum of each MNO countrywide. By varying the impact of the CCI and the spectrum reuse, extensive numerical and simulation results and analyses have been carried out for an example scenario of a country consisting of four MNOs, i.e., MNO 1, MNO 2, MNO 3, and MNO 4 with a subscriber base of, respectively, 40%, 30%, 20%, and 10% of the total countrywide subscribers.

It has been shown that the proposed technique with no CCI provides 2.5 times higher average capacity, SE, EE, and CE performances than that with the maximum CCI. Furthermore, with regard to the SLSA, the proposed technique improves the average capacity, SE, EE, and CE of MNO 1 by 300%, 165%, 75%, and 60%, respectively, with no CCI. The improvement factors, however, decrease as CCI increases and reaches the minimum value when CCI is the maximum. Besides, the required SE and EE for 6G can be achieved by changing either vertical RF ω_{FL} or horizontal RF L such that their product, i.e., ($\omega_{\text{FL}} \times L$), defines the achievable SE and EE performances. Further, the impact of CCI can be compensated by adjusting either vertical RF or horizontal RF. Furthermore, it has been shown that the proposed CoMSAR technique can satisfy both the SE of 370 bps/Hz and EE of 0.3 µJ/bit for 6G mobile systems by reusing the countrywide 28 GHz mmWave spectrum to small cells of MNO 1 of about 61.2% less number of single-floor buildings with no CCI, whereas 6.4% less number of single-floor buildings with the maximum CCI, than that required by the traditional SLSA technique. Lastly, we have discussed the benefits of the proposed technique and pointed out a number of issues as part of further studies on the proposed CoMSAR technique.

APPENDIX A

TABLE A1. LIST OF ACRONYMS/ABBREVIATIONS

Acronym/ Abbreviation	Definition
3D	3-Dimensional
6G	Sixth-Generation
BS	Base Station
CCI	Co-Channel Interference
CE	Cost Efficiency
CoMSAR	Countrywide Millimeter-wave Spectrum Allocation and Reuse
EE	Energy Efficiency
FFR	Fractional Frequency Reuse

ISD	Inter-Site Distance
LOS	Line-Of-Sight
mmWave	Millimeter-Wave
MNO	Mobile Network Operator
NLOS	Non-Line-Of-Sight
NRA	National Regulatory Agency
PBS	Picocell Base Station
RB	Resource Block
SBS	Small Cell Base Station
SE	Spectral Efficiency
SLSA	Static Licensed Spectrum Allocation
TTI	Transmission Time Interval
UE	User Equipment

TABLE A2. LIST OF SELECTED NOTATIONS

Notation	**Description**
t	Index of a TTI
T	Simulation run time with the maximum time of Q
O	Number of MNOs of a country
o	Index of an MNO
M	Amount of mmWave spectrum per MNO in SLSA
l	Index of a building
L	Number of buildings per macrocell
i	Index of an RB
P_{MC}, P_{PC}, and P_{SC}	The transmission power of a macrocell, a picocell, and a small cell, respectively, of an MNO o
ω_{FL}	Number of floors in a building
ω_{fl}	Index of a floor in a building
$M_{\mathrm{C,max}}$	Countrywide mmWave spectrum in RBs
t_{rnw}	Licensed renew term
$S_{\mathrm{F},o}$	Number of SBSs in any building l for an MNO o
ε_{C}	Cost of the countrywide 28 GHz mmWave spectrum $M_{\mathrm{C,max}}$
ε_{o}	Spectrum licensing fee paid by an MNO o
$N_{o,t_{\mathrm{rnw}}}$	Number of subscribers of an MNO o at term t_{rnw}
$N_{\mathrm{C,\,max},t_{\mathrm{rnw}}}$	Number of subscribers of a country at term t_{rnw}
$M_{o,t_{\mathrm{rnw},t}}^{l,\omega_{fl}}$	The optimal amount of licensed spectrum in RBs for an MNO o on any floor ω_{fl} in a building l in TTI t at term t_{rnw}
$\sigma_{t,i,o}^{t_{\mathrm{rnw}}}(\cdot)$	A link throughput at RB=i in TTI=t for an MNO o at t_{rnw} in bps per Hz
$\rho_{t,i,o}^{t_{\mathrm{rnw}}}(\cdot)$	A link SINR at RB=i in TTI=t for an MNO o at t_{rnw} in dB
$M_{\mathrm{MBS},o}$	Spectrum in RBs of a macrocell for an MNO o
$\sigma_{\mathrm{FD,cap},O}^{\mathrm{sys},t_{\mathrm{rnw}}}(\cdot)$, $\sigma_{\mathrm{FD,SE},O}^{\mathrm{sys},t_{\mathrm{rnw}}}(\cdot)$, $\sigma_{\mathrm{FD,EE},O}^{\mathrm{sys},t_{\mathrm{rnw}}}(\cdot)$, and $\varsigma_{\mathrm{FD,CE},O}^{\mathrm{sys},t_{\mathrm{rnw}}}$	System-level average capacity, SE, EE, and CE, respectively, for all MNOs O countrywide at t_{rnw} for l=L when employing the proposed technique
$\sigma_{\mathrm{SLSA,cap},O}^{\mathrm{sys},t_{\mathrm{rnw}}}(\cdot)$, $\sigma_{\mathrm{SLSA,SE},O}^{\mathrm{sys},t_{\mathrm{rnw}}}(\cdot)$, $\sigma_{\mathrm{SLSA,EE},O}^{\mathrm{sys},t_{\mathrm{rnw}}}(\cdot)$, and $\varsigma_{\mathrm{SLSA,CE},O}^{\mathrm{sys},t_{\mathrm{rnw}}}$	System-level average capacity, SE, EE, and CE, respectively, for all MNOs O countrywide at t_{rnw} for l=L when employing SLSA
$\varsigma_{\mathrm{cap},O,\mathrm{IF}}^{\mathrm{sys},t_{\mathrm{rnw}}}$, $\varsigma_{\mathrm{SE},O,\mathrm{IF}}^{\mathrm{sys},t_{\mathrm{rnw}}}$, $\varsigma_{\mathrm{EE},O,\mathrm{IF}}^{\mathrm{sys},t_{\mathrm{rnw}}}$, and $\varsigma_{\mathrm{CE},O,\mathrm{IF}}^{\mathrm{sys},t_{\mathrm{rnw}}}$	Improvement factors in average capacity, SE, EE, and CE, respectively, due to applying the proposed technique

REFERENCES

[1] R. K. Saha, “A Massive Millimeter-Wave Spectrum Allocation and Exploitation Technique Toward 6G Mobile Networks,” Proc. the Fifteenth International Conference on Systems and Networks Communications (ICSNC), Oct. 2020, pp. 32-41.

[2] A. M. Foster, “Spectrum Sharing,” Proc. International Telecommunication Union, the 8th Global Symposium for Regulators, 11-13 March 2008.

[3] R. K. Saha, “Approaches to Improve Millimeter-Wave Spectrum Utilization Using Indoor Small Cells in Multi-Operator Environments Toward 6G,” IEEE Access, vol. 8, pp. 207643-207658, 2020, doi: 10.1109/ACCESS.2020.3037684

[4] X. Yan, S. Qijun, Z. Hongshun, and S. Lulu, “Dynamic Spectrum Allocation Based on Cognitive Radio,” Proc. The 2009 5th Asia-Pacific Conference on Environmental Electromagnetics, Sep. 2009, pp. 254-257.

[5] Z. Wei, D. Yang, and L. Sang, “Dynamic System Level Frequency Spectrum Allocation Scheme Based On Cognitive Radio Technology,” China Commun., vol. 11, no. 7, pp. 84-91, Jul. 2014.

[6] H. Shajaiah, A. Khawar, A. Abdel-Hadi, and T. C. Clancy, “Resource Allocation with Carrier Aggregation in LTE Advanced Cellular System Sharing Spectrum with S-Band Radar,” Proc. IEEE Int. Symp. Dyn. Spectr. Access Netw. (DYSPAN), Apr. 2014, pp. 34-37.
[7] F. Liu, D. Zhang, L. Yue, F. Gao, and R. Du, “An OFDM Multi-User Spectrum Resource Allocation Algorithm Based on Joint Access Mechanism,” Proc. of the IEEE 9th Int. Conf. Softw. Eng. Service Sci. (ICSESS), Nov. 2018, pp. 589-592.
[8] H. Kim, Y. Lee, and S. Yun, “A Dynamic Spectrum Allocation Between Network Operators with Priority-Based Sharing and Negotiation,” Proc. The 2005 IEEE 16th International Symposium on Personal, Indoor and Mobile Radio Communications, Sep. 2005, pp. 1004-1008.
[9] S. J. Kim, E. C. Kim, S. Park, and J. Y. Kim, “Dynamic Spectrum Allocation with Variable Bandwidth for Cognitive Radio Systems,” Proc. the 2009 9th International Symposium on Communications and Information Technology, Sep. 2009, pp. 106-109.
[10] J. Gu, “Dynamic Spectrum Allocation Algorithm for Resolving Channel Conflict in Cognitive Vehicular Networks,” Proc. 7th IEEE Int. Conf. Electron. Inf. Emergency Commun. (ICEIEC), Jul. 2017, pp. 413-416.
[11] N. N. Bhuiyan, R. T. Ratri, I. Anjum, and M. A. Razzaque, “Traffic-Load Aware Spectrum Allocation in Cloud Assisted Cognitive Radio Networks,” Proc. the IEEE Region 10 Humanitarian Technol. Conf. (R10-HTC), Dec. 2017, pp. 598-601.
[12] R. K. Saha and C. Aswakul, “A Tractable Analytical Model for Interference Characterization and Minimum Distance Enforcement to Reuse Resources in Three-Dimensional In-Building Dense Small Cell Networks,” International Journal of Communication Systems, vol. 30, Art. No. e3240, Jul. 2017, doi.org/10.1002/dac.3240
[13] R. K. Saha, “Modeling Interference to Reuse Millimeter-Wave Spectrum to In-Building Small Cells Toward 6G,”' Proc. IEEE VTC-Fall, Nov. 2020, pp. 1-6.
[14] N. Saquib, E. Hossain, and D. Kim, “Fractional Frequency Reuse for Interference Management in LTE-Advanced Hetnets,” IEEE Wireless Communications, vol. 20, pp. 113-122, Apr. 2013, doi: 10.1109/MWC.2013.6507402.
[15] R. A. Hassan, A. Idris, H. Adto, M. Ramadhan, and M. Kassim, “Reduction of Inter-Cell Interference in Close Proximity Cell Using Dynamic Fractional Frequency Reuse Method,” Proc. IEEE Conf. Syst., Process Control (ICSPC), Dec. 2017, pp. 157-161.
[16] R. K. Saha, “A Technique for Massive Spectrum Sharing with Ultra-Dense In-Building Small Cells in 5G Era,” Proc. the 2019 IEEE 90th Vehicular Technology Conference (VTC2019-Fall), Sep. 2019, pp. 1-7.
[17] P. Yen, Q. Zhan, and H. Minn, “New Fractional Frequency Reuse Patterns for Multi-Cell Systems in Time-Varying Channels,” IEEE Wireless Commun. Lett., vol. 4, no. 3, pp. 253-256, Jun. 2015.
[18] S. C. Lam, R. Subramanian, K. Sandrasegaran, P. Ghosal, and S. Barua, “Performance of well-known frequency reuse algorithms in LTE downlink 3GPP LTE systems,” Proc. the 9th Int. Conf. Signal Process. Commun. Syst. (ICSPCS), Dec. 2015, pp. 1-5.
[19] R. K. Saha, “A Hybrid Interweave-Underlay Countrywide Millimeter-Wave Spectrum Access and Reuse Technique for CR Indoor Small Cells in 5G/6G Era,” Sensors, vol. 20, Art. No. 3979, 2020, doi.org/10.3390/s20143979.
[20] R. K. Saha, “On Exploiting Millimeter-Wave Spectrum Trading in Countrywide Mobile Network Operators for High Spectral and Energy Efficiencies in 5G/6G Era,” Sensors, vol. 20, Art. No. 3495, 2020, doi.org/10.3390/s20123495.
[21] R. K. Saha, “3D Spatial Reuse of Multi-Millimeter-Wave Spectra by Ultra-Dense In-Building Small Cells for Spectral and Energy Efficiencies of Future 6G Mobile Networks,” Energies, vol. 13, Art. No. 1748, 2020, doi.org/10.3390/en13071748.
[22] R. K. Saha “Spectrum allocation and reuse in 5G new radio on licensed and unlicensed millimeter-wave bands in indoor environments,” Mobile Information Systems, vol. 2021, art. ID 5538820, pages 21, 2021, doi: 10.1155/2021/553882
[23] R. Allan, “Application of FSS Structures to Selectively Control the Propagation of Signals into and Out of Buildings – Executive Summary,” ERA Technology Ltd, Cleeve Road, Leatherhead Surrey, KT22 7SA UK. Available online: https://www.ofcom.org.uk/__data/assets/pdf_file/0020/36155/exec_summary.pdf [retrieved: Feb. 2020]
[24] Propagation Data and Prediction Methods for The Planning of Indoor Radiocommunication Systems and Radio Local Area Networks in The Frequency Range 300 MHz to 450 GHz. Recommendation ITU-R P.1238-10, 08/2019. Available online: https://www.itu.int/rec/R-REC-P.1238 [retrieved: Feb. 2020]
[25] D. Lu and D. Rutledge, “Investigation of Indoor Radio Channels from 2.4 GHz to 24 GHz,” Proc. IEEE Antennas and Propagation Society International Symposium. Digest. Held in conjunction with: USNC/CNC/URSI North American Radio Sci. Meeting (Cat. No.03CH37450), Jun. 2003, pp. 134-137.
[26] R. K. Saha, S. Nanba, and K. Nishimura, “A Technique for Cloud Based Clustering and Spatial Resource Reuse and Scheduling of 3D In-Building Small Cells Using CoMP for High Capacity CRAN,” IEEE Access, vol. 6, pp. 71602-71621, Nov. 2018, doi: 10.1109/ACCESS.2018.2879835.
[27] H. A. U. Mustafa, M. A. Imran, M. Z. Shakir, A. Imran, and R. Tafazolli, “Separation Framework: An Enabler for Cooperative and D2D Communication for Future 5G Networks,” IEEE Commun. Surveys Tuts., vol. 18, no. 1, pp. 419-445, 1st Quart., 2016, doi: 10.1109/COMST.2015.2459596.
[28] Q. Cui, H. Song, H.Wang, M. Valkama, and A. A. Dowhuszko, “Capacity Analysis of Joint Transmission Comp with Adaptive Modulation,”' IEEE Trans. Veh. Technol., vol. 66, no. 2, pp. 1876-1881, Feb. 2017, doi: 10.1109/TVT.2016.2564106.
[29] J. D. Chimeh, M. Hakkak, and S. A. Alavian, “Internet Traffic and Capacity Evaluation in UMTS Downlink,” Proc. the Future Generation Communication and Networking (FGCN), Dec. 2007, pp. 547-552.
[30] L. Kleinrock, “Queueing Systems: Theory,” vol. 1. Hoboken, NJ, USA: Wiley, 1975.
[31] R. K. Saha, “A Hybrid System and Technique for Sharing Multiple Spectrums of Satellite Plus Mobile Systems with Indoor Small Cells in 5G and Beyond Era,” IEEE Access, vol. 7, pp. 77569-77596, 2019, doi: 10.1109/ACCESS.2019.2921723.
[32] R. K. Saha and C. Aswakul, “A Novel Frequency Reuse Technique for In-Building Small Cells in Dense Heterogeneous Networks,” IEEJ Transactions on Electrical and Electronic Engineering, vol. 13, pp. 98-111, Jan. 2018, doi.org/10.1002/tee.22503.
[33] Evolved Universal Terrestrial Radio Access (E-UTRA); Radio Frequency (RF) System Scenarios. document 3GPP TR 36.942, V.1.2.0, 3rd Generation Partnership Project, Jul. 2007. Available online: https://portal.3gpp.org/ desktopmodules /Specifications/ Specification Details.aspx?specificationId=2592 [retrieved: Feb. 2020]
[34] Simulation Assumptions and Parameters for FDD HeNB RF Requirements. document TSG RAN WG4 (Radio) Meeting #51, R4-092042, 3GPP, May 2009. Available online:

https://www.3gpp.org/ftp/tsg_ran /WG4_Radio/TSGR4_51/Documents/ [retrieved: Feb. 2020]

[35] Guidelines for Evaluation of Radio Interface Technologies for IMT-2020. Report ITU-R M.2412-0 (10/2017), Geneva, 2017. Available online: https://www.itu.int/dms_pub/itu-r/opb/rep/R-REP-M.2412-2017-PDF-E.pdf [retrieved: Feb. 2020]

[36] R. K. Saha, P. Saengudomlert, and C. Aswakul, "Evolution Toward 5G Mobile Networks-A Survey On Enabling Technologies," Engineering Journal, vol. 20, pp. 87-119, Jan. 2016, doi.org/10.4186/ej.2016.20.1.87.

[37] G. R. Maccartney, T. S. Rappaport, S. Sun, and S. Deng, "Indoor Office Wideband Millimeter-Wave Propagation Measurements and Channel Models at 28 and 73 GHz for Ultra-Dense 5G Wireless Networks," IEEE Access, vol. 3, pp. 2388-2424, 2015, doi: 10.1109/ACCESS.2015.2486778.

[38] R. K. Saha, "Spectrum Sharing in Satellite-Mobile Multisystem Using 3D In-Building Small Cells for High Spectral and Energy Efficiencies in 5G and Beyond Era," IEEE Access, vol. 7, pp. 43846-43868, Mar. 2019, doi: 10.1109/ACCESS.2019.2908203.

[39] Z. Zhang, Y. Xiao, Z. Ma, M. Xiao, Z. Ding, X. Lei, G. K. Karagiannidis, and P. Fan, "6G Wireless Networks: Vision, Requirements, Architecture, and Key Technologies," IEEE Vehicular Technology Magazine, vol. 14, pp. 28-41, Sep. 2019, doi: 10.1109/MVT.2019.2921208.

[40] S. Chen, Y. C. Liang, S. Sun, S. Kang, W. Cheng, and M. Peng, "Vision, Requirements, and Technology Trend of 6G: How to Tackle the Challenges of System Coverage, Capacity, User Data-Rate and Movement Speed," IEEE Wireless Communications, vol. 27, no. 2, pp. 218-228, Apr. 2020, doi: 10.1109/MWC.001.1900333.

[41] C.-X. Wang, F. Haider, X. Gao, X.-H. You, Y. Yang, D. Yuan, H. M. Aggoune, H. Haas, S. Fletcher, and E. Hepsaydir, "Cellular Architecture and Key Technologies for 5G Wireless Communication Networks," IEEE Communications Magazine, vol. 52, pp. 122-130, Feb. 2014, doi: 10.1109/MCOM.2014.6736752.

[42] G. Auer, V. Giannini, C. Desset, I. Godor, P. Skillermark, M. Olsson, M. A. Imran, D. Sabella, M. J. Gonzalez, O. Blume, and A. Fehske, "How Much Energy is Needed to Run a Wireless Network?" IEEE Wireless Communications, vol. 18, pp. 40-49, Oct. 2011, doi: 10.1109/MWC.2011.6056691.

[43] R. K. Saha and C. Aswakul, "Incentive and Architecture of Multi-Band Enabled Small cell and UE for Up-/Down-link and Control-/User-plane Splitting for 5G Mobile Networks," Frequenz Journal of RF-Engineering & Telecommunications, vol. 71, no. 1-2, pp. 95-118, Jan. 2017, doi: 10.1515/FREQ-2016-0014.

MAC and Network Layer Solutions for Underwater Wireless Sensor Networks

Anne-Lena Kampen
Western Norway University of Applied Sciences (HVL)
Bergen, Norway
e-mail: Anne-Lena.Kampen@hvl.no

Roald Otnes
Norwegian Defence Research Establishment (FFI)
Horten, Norway
e-mail: Roald.Otnes@ffi.no

***Abstract*—The underwater acoustic environment poses challenges for communication that can make solutions from terrestrial radio networks ineffective. However, the mature terrestrial solutions are based on decades of real-world research and experience, proving their sustainability and reliability. Although not suitable for direct replication, it may be wise to take advantage of these proven solutions. With this in mind, it is valuable to study successful terrestrial approaches and evaluate their ability to support the harsh underwater environment, and to assess how procedures and algorithms can be adapted for efficient underwater communication. In this paper, we revisit frequently used Medium Access Control (MAC) protocols and discuss the challenges they face in the underwater environment. In addition, underwater challenges related to multi-hop data collection are discussed. To improve reception reliability in the highly dynamic underwater environment, we focus on broadcast solutions that are constrained to avoid network flooding. Location-based techniques are promising in this regard. Related to the MAC layer, underwater communication solutions should focus on preventing collisions at receiver, and reducing the time between packet receptions. Furthermore, machine learning techniques can give more intelligent and accurate decisions, and may provide more autonomous network operations. These techniques should be further investigated.**

Keywords-UWSN; underwater wireless sensor networks; Medium Access Control MAC; underwater routing, survey.

I. INTRODUCTION

Underwater wireless sensor networks (UWSNs) can provide extended connectivity for applications within underwater environmental monitoring, oil and gas industry, offshore wind, and defense purposes. The topic is given weight in the Norwegian Research Council funded research-based innovation center “Smart Ocean”, motivating the present survey paper which discusses the state of the art in UWSN research and which approaches can and cannot be transferred from terrestrial radio networks.

UWSNs consist of nodes deployed underwater that use wireless communication to generate a connected network. The ‘last mile’ in these underwater networks is to transport the collected data to the surface for further transmission toward a destination using terrestrial technologies. Focusing on the underwater network, the protocols used may borrow ideas from well-known terrestrial solutions. However, they must be thoroughly assessed against the unique characteristics of the underwater environment as discussed in [1], and further elaborated in this paper.

The United Nation (UN) sustainability goal #14, life below water [2], calls for underwater surveillance solutions to monitor the marine environment and strengthen ecosystem knowledge. To this end, sensor networks can be essential building-blocks in systems used by the ocean industries and public surveys for monitoring the seabed and water-column conditions. The network can contribute to sustainable exploitation of underwater resources by monitoring environmental parameters, and ensure responsible growth with well-controlled environmental impact.

The discussion is focused toward wireless networks. Using wired communication in underwater environments would increase the available bandwidth and provide more reliable communication. However, installation of a wired network consumes significant time and resources, and the network is less scalable due to fixed physical connections. In addition, fishing activities and underwater currents can move and twist nodes, cables, and mechanical junctions such that the communication infrastructure is deteriorated or is cut off.

Sustainable network operation relies upon well-suited Medium Access Control (MAC) and network layer protocols. The goal of the MAC is to wisely share the network media between the nodes to provide efficient data collection. The network layer enables data from remote nodes to reach its destination. The protocols must adapt to the environmental challenges related to the underwater media, such as low propagation speed, low and dynamic channel capacity, interference, ambient noise, and asymmetric links, and so forth. In addition, the sensors are mainly battery operated, and battery replacement is unfeasible. Furthermore, the characteristics of the propagation environment may change substantially, both on short and long timescales. Thus, the protocols should provide solutions that cope with the dynamic environments and, simultaneously, reduce the energy consumption of the nodes.

Current underwater wireless solutions are mainly based on underwater acoustic transmission [3]. The signal propagation for acoustic underwater communication is five orders of magnitude slower than the speed of light; in addition, it is affected by temperature, salinity and depth [4, 5]. The low propagation speed presents a fundamental challenge in coordinating the access to the shared communication medium. The time window used by the resource reservation processes should be compressed to allow more time for payload.

Network layer protocols establish routing paths to enable multihop transmission, which can be used to increase the area covered by the network and/or to reduce the output power, i.e., reduce transmission range, and save energy. The routing paths are formed based on specified criteria that aim to support the overall goal for the communication and/or to support overall network goals. For instance, the data can be transmitted over several paths simultaneously to support reliable communication, or the data can be sent alternately over different available paths to balance the energy consumption in the network to prevent early depletion of nodes. However, due to the dynamic characteristic of the channel, and potential movement of sensor nodes, it is difficult to construct proactive routing paths, while reactive paths introduce high transmission delay. On the contrary, broadcasting can limit the delay and reduce the need for proactive configuration. In addition, the reliability is improved because the data are transmitted over several paths. However, the broadcast should be constrained to reduce network traffic and limit the energy consumption of the nodes.

Table 1 compares characteristics that are important with respect to MAC and network layer protocol performance. The peculiar characteristics of the underwater environment mean that protocols used in terrestrial communication require adjustments to provide efficient underwater communication. To this end, the contribution of this paper is to discuss characteristics that are challenging when converting basic terrestrial MAC layer protocols for use in the underwater environment. In addition, network layer protocols that enable constrained multicast are investigated. Basic multicast should be avoided to prevent excessive network traffic as well and excessive energy consumption. Researchers and developers might find our discussion valuable, as it presents general arguments that should be considered during protocol development and evaluation.

There are several key performance indicators that can be used to assess solutions underwater communication. Energy consumption is an important indicator. Reducing the consumption increases the network lifetime, which is crucial since the nodes are generally battery charged, and battery replacement is expensive and not very feasible due to the harsh environmental condition. Other important indicators are throughput, reliability, latency and access-delay. In addition, the solution must be adaptable to the dynamic underwater environment.

The rest of the paper is structured as follows. In Section II we present related work. MAC layer protocols and their issues related to the underwater environment are discussed in Section III. Network layer protocols, and their issues, are discussed in Section IV. Software Defined Network (SDN) and Machine Learning (ML) is shortly discussed in Section V. In Section VI network optimization is discussed in the light of modem and environmental characteristics. In Section VII we present conclusions.

II. RELATED WORK

The increasing interest in life and resources below water has mobilized a wide range of research on underwater sensor networks. The communication protocols are important to enable efficient operation. Thus, a range of solutions are suggested in the literature, and various surveys present and discuss selected solutions focusing on various aspects. A thorough discussion of MAC protocols for underwater acoustic networks is found in [6]. It is emphasized that further studies should focus on methods that handle the long propagation delay in ways that improve the utilization of the available bandwidth, for instance by allowing concurrent transmission as long as packet collision at the receiver is prevented. The MAC survey presented in [7] points out that current MAC protocols designed for terrestrial solutions are not suitable for underwater communication, and introduces software-based approaches as a promising solution to address the challenges of underwater networks. Boukerche and Sun [8] discuss underwater channel modeling, MAC and routing protocols, and localization schemes. It is pointed out that the underwater environment is much more complex than the hypotheses that existing approaches are commonly based upon. The complex environmental characteristics are the reason that we, for network layer solutions, focus on constrained broadcast rather than single path solutions that are more vulnerable for changing channel characteristics.

Table 1 Comparing terrestrial and underwater characteristics.

	Terrestrial	Underwater acoustic
Propagation speed	Almost the speed of light, $3*10^8$ m/s	About $1.5*10^3$ m/s in seawater
Propagation delay between different nodes	Almost negligible.	Depends on distance betweeen nodes.
Data rate	High	Low
Channel quality	High	Low and dynamic

Khisa and Moh [9] focus on energy-efficient routing protocols. Energy consumption is also very much in focus when Khalid et al. discuss localization-based and localization-free routing protocols, along with routing issues, in [10]. They conclude by pointing out that all protocols have pros and cons, so that a protocol that is best for all cases cannot be found. The same is pointed out in [11], where routing protocols for acoustic sensor networks are assessed according to feasible application scenarios. An earlier survey that gives a nice overview of routing protocols and network issues is presented in [12]. Terrestrial routing protocols are also compared with Underwater Wireless Sensor Networks (UWSNs) in the survey. The survey presented in [13] focuses on cross-layer designed routing protocols. The authors define cross layer design as a design where algorithms from different layers can exchange information with each other, and point out that layered designs are better for creating adaptive solutions. A substantial part of the protocols suggested for UWSNs do, at least to some degree, follow the definition of cross-layer solutions defined in the paper. For instance, using this definition, all network layer protocols that use location or energy level as selection criteria will be categorized as cross-layer protocols.

Our focus is to present the issues that affect the MAC and network layer protocols. We review traditional MAC layer algorithms and describe their weaknesses related to underwater communication. At the network layer, the focus is on methods that reduce broadcast. Due to the dynamic environment, the links are very unreliable. Broadcast communication is therefore advantageous compared to communication over predetermined dedicated links. However, simple broadcast (flooding) is a waste of energy.

III. MAC PROTOCOLS

MAC protocols have a large impact on the overall network performance, because they coordinate the nodes' access to the medium. The access must be shared fairly between the nodes, the scarce bandwidth resources must be efficiently utilized, the access delay must be limited, and packet collisions should be minimized. To avoid collisions, transmission time as well as packet length must be taken into consideration. That is, the transmission time between the sender and the node that is farthest away, but still within the sender's transmission range (interference range), must be considered. In addition, sustainable MAC protocol solutions require energy-efficient operations that lengthen the network lifetime and reduce the management cost. To this end, the impact for the various states of the communication processes must be investigated to develop the most optimal solution. In addition, dynamic environments and low channel capacity require adaptive and bandwidth-efficient protocols.

The access methods generally used can be categorized as fixed-assignment protocols, demand-assigned protocols and random-access protocols [14]. In fixed-assignment protocols, the channel is divided between the nodes so they can access the medium without any risk of collisions. Typical protocols used are Time Division Multiple Access (TDMA), Frequency Division Multiple Access (FDMA), and Code Division Multiple Access (CDMA). These protocols provide predictable access delay, and efficient utilization of available bandwidth. In addition, no energy is wasted on collisions. However, the assigned resources require signaling to renegotiate resources when the network topology changes or if nodes require more resources due to increased traffic load. In addition, the dynamic underwater environment means that the quality of pre-allocated resources can fluctuate, causing issues related to packet loss and throughput.

Demand-assigned protocols provide short term channel assignments. Polling schemes belong to this class of protocols. The nodes may emit request for channel allocation, and successful allocation is confirmed back to the nodes with description of the allocated resources. The resources may be defined in terms of number and positions of TDMA slots. Time slotted communication is illustrated in Figure 1. The administration of resources can be distributed to some key nodes in the network, for instance to cluster heads in clustered networks. However, network-wide resource reservation is complex as traffic from nodes in adjacent areas can interfere. Furthermore, efficient TDMA requires precise synchronization, which is challenging in underwater environments due to the long and variable transmission delay. In addition, using guard times that are adjusted to allow different time delays and time references will lead to inefficient utilization of the channel. However, short periods of static and predictable propagation delays may provide synchronization that is accurate enough [15].

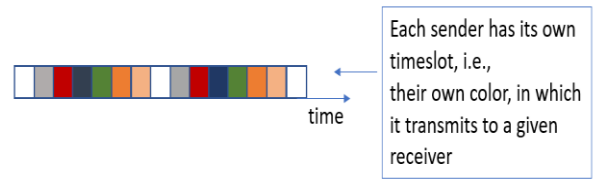

Figure 1. Time slotted communication. TDMA

The nodes in random-access protocols are uncoordinated and operate in a fully distributed manner. ALOHA is one of the earliest and most important protocols in this category. In the simplest version of ALOHA, the nodes transmit the packets as soon as they are generated. Successfully receiving the packet, the receiver transmits an Acknowledgement packet (ACK) back to the sender. If the sender does not receive ACK, it assumes that a collision has occurred. It waits a random amount of time (backoff) before retransmitting the packet. ALOHA works well when the traffic load is low. Under heavier load the number of collisions increases, increasing the delay and energy consumption, and reducing the throughput efficiency. In slotted ALOHA, the time is divided into timeslots, and packet transmission can only start at the beginning of a timeslot. The slot time is long enough to accommodate the longest allowed packets. Thus, only simultaneously transmitted packets can collide. However, because of the long transmission delay, this is not true in underwater communication. In addition, to avoid collisions, the slot length must also take the transmission delay as well as packet length into consideration.

Another popular random-access protocol is Carrier Sense Multiple Access with Collision Avoidance (CSMA/ CA), which is a random-access scheme with carrier sense and collision avoidance through random backoff. Different backoff algorithms can be used, but they roughly follow the following procedure: To avoid disrupting ongoing transmissions the nodes listen (carrier sense) to the channel, and choose a random number of backoff slots within a contention window. After the channel has been idle for a time interval denoted Distributed Interface Space (DIFS), the backoff value is decremented for each idle timeslot observed on the channel. As soon as the counter expires, the node accesses the medium. See illustration in Figure 2, where node A transmits a packet after the channel has been idle for DIFS plus the time it takes for the backoff value to be counted down. Node B has to wait until the channel has been idle for DIFS before it starts counting down the backoff value. A collision triggers retransmission with a new random selection of backoff time, and for each collision the contention window doubles. This is called exponential backoff. Using slotted CSMA, the backoff equals a random integer number of timeslots. However, due to the time-delay

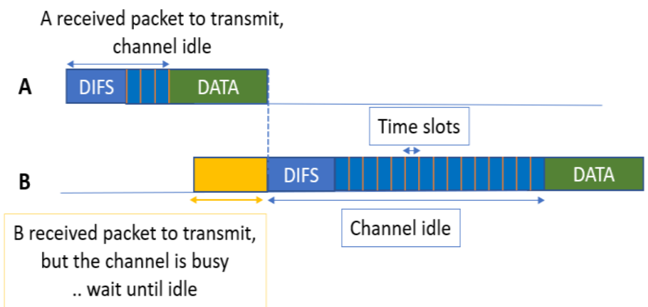

Figure 2. Carrier Sense Multiple Access CSMA

variations in underwater environments, unslotted version could be more feasible. An explicit ACK is sent by the receiver upon successful reception of the packet. Asymmetric links affect the communication efficiency especially when reliable communication is required. The reason is that when ACK messages are lost, the packets will be re-transmitted. Re-transmitted packets increase network traffic, which increases collision probability and also the energy consumption.

Furthermore, carrier-sense protocols are susceptible to the hidden-node problem and unfair access. The slow propagation speed can lead to unfair access since there is bias in estimating clear channel: Nodes close to the signal source get a clear channel earlier, providing them with more access opportunities [16].

The hidden-node problem is caused by the different location of the sender and the receiving node, see Figure 3. A transmitting node, N_1, cannot detect activity at the receiver, N_2, that is caused by a sending node, N_3, whose transmission reaches the receiver, but not the node N_1. To reduce the hidden-node problem, Request To Send/Clear To Send (RTS/CTS) can be used. After the sending node has obtained channel access it sends an RTS packet to the receiver. The packet includes a time field that indicates the duration of the overall transaction. Successfully receiving the RTS means that there are no hidden nodes that are currently creating interference at the receiver side. The sender replies with an CTS, which also includes the duration time field. Receiving the CTS, the transmitter starts transmitting the data packet. The hidden-node problem is reduced since both the sender, by means of the RTS, and the receiver, by means of the CTS, have informed their neighbors about the upcoming transmission. However, a spatial unfairness may occur since nodes closer to the receiver may always win Request To Send (RTS) contentions because their requests are always received earliest [17].

To account for the long transmission delays in the underwater environment, the nodes must delay data transmission according to the longest possible delay, and the relatively long time span increases the probability of transmission from a neighboring node. Thus, basic access control processes, such as carrier sense, reservation of the media, and ACK are more time-consuming, and more management is required if these processes are to be optimized for neighbors at different distances.

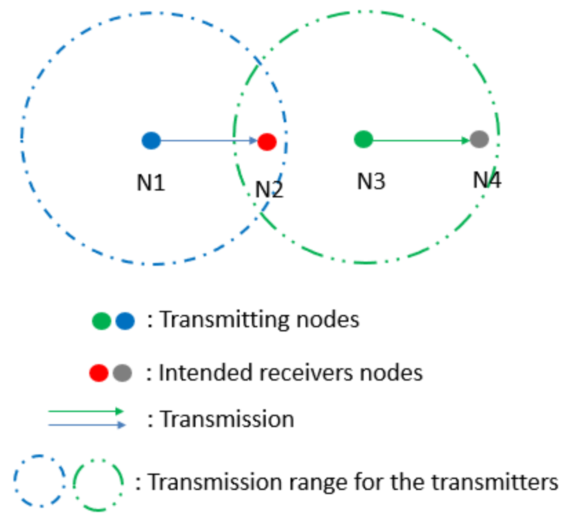

Figure 3. Hidden node

Channel utilization is reduced because collision-free reception is not guaranteed although the transmissions from different nodes are collision-free. Likewise, concurrent transmission may not lead to collision [18]. To improve the media utilization, receiver-centric solutions can be used to handle the unequal delay that exists between the various transmitting nodes. Receivers can arrange the transmission time for the transmitters so that collisions are avoided, while avoiding that the time between each received packet is unnecessarily long, such as suggested in [19]. The major challenge of the solution is prediction and management of delays, which require frequent information exchange between nodes, especially under dynamic channel conditions.

No solution can take all challenges into account. Thus, no solutions fit all scenarios as confirmed in the at-sea-experiment presented in [20], where the performance of three well-known MAC layer protocols, namely CSMA, T-Lohi [21, 22], and Distance Aware Collision Avoidance Protocol (DACAP), is evaluated in an extensive sea-test during at-sea campaigns. CSMA is the simplest of these protocols, where, to prevent collisions, the nodes listen to detect if the media is idle before transmission. If not idle, the nodes back off according to an exponential back-off mechanism after which they again listen for a silent channel. ACK can be used for reliable communication. Applying T-Lohi, the node transmits a reservation tone, after which it listens to the channel for the duration of a Contention Round (CR). If no other tones are heard during CR, the data packet is transmitted. Otherwise, it enters back-off state for a random number of CR before repeating the procedure. The most advanced of the three protocols is DACAP, in which RTS/CTS is used to reserve the channel. To warn about possible interference, the destination node sends a short warning packet to its sender if it overhears control packets from other nodes after sending its CTS and before receiving the associated data packet. If the sender overhears a control packet, or receives a warning from its destination while waiting for CTS, it aborts data communication.

Using two different modems, the results reported in [20] for the three different MAC protocols show similar trends, although the overall protocol performance is significantly affected by the delays and overheads associated with the acoustic modem used. Furthermore, the results presented show that different traffic loads, channel conditions, and evaluation metrics call for different solutions. Basically, solutions should be able to adapt, in a distributed way, to dynamically changing conditions. Using DACAP, the network performance is deteriorated when the traffic load is increased. ACK packets improve packet delivery ratio as long as the link is symmetric, however this is not always the case. CSMA reduces the transmission attempts since the channel is reserved by the data packet itself, however, the whole packet has to be retransmitted when collisions occur. The end-to-end delay of CSMA and DACAP use exponential backoff, making the delay increase rapidly with increased number of retransmissions. Not using exponential backoff, T-Lohi has lower end-to-end delay, the price paid is higher packet loss.

In contrast to single-channel protocols discussed so far, multiple-channel protocols rely on several channels for communication to increase network throughput, reduce channel access delay, and potentially save energy. Neighboring nodes can communicate simultaneously, provided that they communicate using unequal data channels. Furthermore, control signals sent on a different channel will not affect the data that are sent.

In [23], the control channel is slotted so each node in a neighborhood is assigned a unique slot. Thus, also control packets are prevented from collisions. The solution suggested in [24] presents quorum-based data channel allocation to prevent collisions. However, generation and management of multichannel protocols is complex, and require advanced modems. In addition, if the nodes are equipped with only one transceiver, it means that they can only work one channel at a time, either on the control channel or on the data channel. When this is the case, handshaking protocols such as RTS/CTS must be tuned to prevent the triple-hidden-node problem [25]. The triple-hidden problem occurs if two of the nodes in a neighborhood are communicating on a data channel. Simultaneously, two other nodes use the control channel for handshaking and agree to use channel A for data communication. The first two nodes will then be unaware of the data channel that the last two nodes selected. Thus, if the first two nodes want to initiate a new communication, they may select data channel A, creating a collision.

Centralized one-hop network solutions simplify media access management and general network complexity at the cost of network coverage and network dynamics. Collisions may be avoided using a polling approach where the nodes are prohibited from transmission unless polled by the central node. The polling sequence is not required to be sequential; it can contain repetitions to support nodes with various amount of sensor data [26]. To approach the throughput gained using TDMA, [27] suggests a centralized approach. The gateway measures the delay to each individual node to organize the nodes' transmission time and sequence. The gateway manages the network operation so the data from all the nodes are received in strict order, resembling a subdivision frame. Although interesting approaches, they require the nodes to stay awake to listen for polling requests. A general weakness of the polling approach is that it relies on symmetric links between the central controller and the other nodes. This is not always the case in underwater communication.

To summarize, there is no single solution that works best in all scenarios, and there is probably a need for solutions that can be adapted to dynamic changes. Furthermore, most of the underwater MAC protocols suggested follow terrestrial approach, trying to avoid transmission collision, although this will not guarantee against collision at reception [6]. To efficiently utilize the scarce bandwidth available underwater, the focus should be on the receiver side. Solutions must reduce the time between packet receptions while simultaneously preventing collisions at the receiver.

IV. NETWORK LAYER PROTOCOLS

Multi-hop communication can be used to increase the area covered by the network, or it can be used to reduce the distance between nodes. The advantage of reducing the distance is that the nodes' output power can be reduced to save energy. Also, the reduced distance can be used to increase the bit rate by increasing the transmission frequency and bandwidth. Furthermore, short distance between nodes increases the granularity of the surveyed area, which may be valuable for picking up local variations and trends related to the parameters surveyed. On the other hand, longer distances between nodes in multi-hop networks can reduce equipment and management costs.

Multihop communication entails challenges such as increased network traffic and imbalance in the energy consumption in the network. Traffic increases because data packets must be forwarded, and management information must be exchanged to generate and maintain the routing paths. Energy imbalance occurs since the nodes in the vicinity of the sink must forward packets for all remotely located nodes. Furthermore, the harsh underwater environment makes the generation of routing paths more challenging. For instance, it is likely that the quality of a substantial amount of the links is time varying, thus proactively generated paths may not be reliable. Reactively created paths, on the other hand, introduce long delay. In addition, the links may be unidirectional or asymmetric, which makes it difficult to utilize paths that may be well-working and stable for communication in the correct direction. Broadcasting alleviates the challenges related to generating routing paths since all candidate paths are tried, and no specific routing paths needs to be generated. However, broadcasting creates excessive traffic as all nodes forward received data packets as illustrated by the blue arrows pointing in both directions in Figure 4. Whichever node generated the data packet, it is flooded throughout the whole network, consuming bandwidth and energy. To prevent this excessive usage of resources, the broadcast should be constrained.

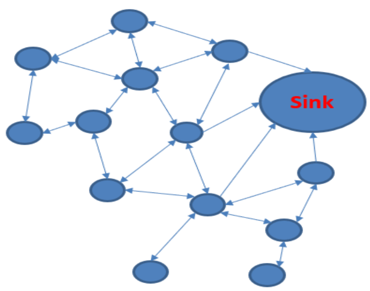

Figure 4. Broadcasting.

Opportunistic routing [28] can be an efficient method to constrain broadcasting. The basic idea is that all receivers contend to forward packets, i.e., the senders broadcast the packets, which are forwarded by the most optimal receiver. Location-based protocols can be used for opportunistic routing in underwater environments. Using a greedy scheme, packets are always forwarded by the node located closest to the sink. This is illustrated in Figure 5, where the green node transmits a packet. The circle around the green node illustrates green node's transmission range. The red node is the destination, i.e., the sink. The orange node is the node inside the green node's transmission range that is closest to the sink. Thus, the orange node forwards the packet. Only local information is used to decide whether the received data should be forwarded, no routing data needs to be exchanged. For instance, each data packet contains information about the destination's location. Nodes that receive the packet start a timer that is proportional to their own distance to the destination. If the node overhears the packet being forwarded by a neighboring node before its own timer reaches zero, it refrains from forwarding the packet. Otherwise, it forwards the packet. The long delay in underwater communication requires that the timer that sets the holding-time (the time between a packet is received until it is potentially forwarded) wisely. Two aspects must be considered. Firstly, the timer must be long enough to ensure that a packet forwarded by a more preferred node is received by the less preferred node before the timer of the less preferred node expires. Due to the underwater environment, it takes time for the forwarded packet to reach the less preferred nodes. Secondly, it is likely that the node in the more preferred location receives the packet later because it is probably located closer to the sink, and further from the transmitter. To sum up: wait until the most-preferred node receives the packet, then wait for the packet relayed by this most-preferred node to reach the less-preferred nodes. Taking both of these aspects into consideration increases the delay in the network. In addition, when the number of potential successor nodes is high, a wide range of distinct holding-time values is required to prevent multiple node timers from expiring simultaneously. To provide a broad range of distinct holding-time values, the average delay in the network increases.

Location-based opportunistic protocols require that nodes know their location. GPS is unfeasible as an underwater location service. One method of solving the underwater location problem is to let some dedicated nodes, with known locations, send out beacons at regular intervals. Based on

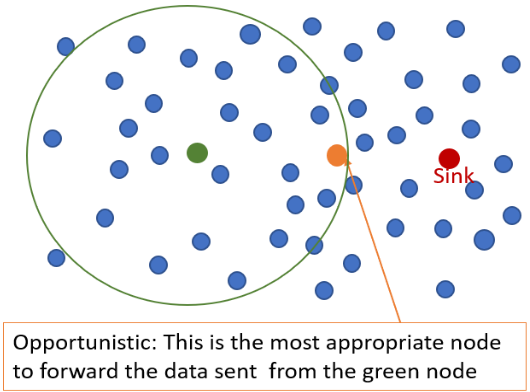

Figure 5. Opportunistic routing.

received signals, other nodes can use methods like triangulation to determine their own location. However, some nodes may be located such that they cannot receive the beacons emitted to estimate locations. To prevent data from these nodes from being lost, a method such as suggested in [29] can be used: The nodes that do not receive location information use a reactive protocol to send data to the best-located neighbor node.

Routing pipe can be used to reduce the number of potential forwarding nodes, and reduce the probability of excessive network traffic for opportunistic protocols. In addition, it alleviates the increased delay needed to accommodate the broad range of distinct holding-time values discussed above. Assuming a vector from the sender to the target node, the routing pipe is a cylinder with adjustable radius centered around that vector. Nodes inside the cylinder are candidate forwarding nodes. The transmitted packet carries the position of the sender node, the target node, and the forwarding nodes to enable the receivers to determine whether they are located inside the routing pipe, and whether they are located closer to the destination than the transmitting node. This is illustrated in Figure 6. The green node transmits a packet toward the sink (the red node). All nodes within the green circle encircling the green node are covered by transmission. The packet is forwarded by the orange node since it is the node inside the pipe (blue shaded cylinder) that is closest to the sink. Adjusting the width of the cylinder, or the transmission range, adjusts the number of candidate forwarders. In [30], to reduce the chances of forwarding data packets, nodes with less energy than the transmitting node intentionally calculate a reduced pipe diameter. Thus, they reduce the chance of being inside the cylinder formed by the sender-receiver vector and diameter. This is done to improve the energy balance in the network.

A challenge related to location-based routing is the possible existence of void regions in the network. To prevent data loss, some measures are needed to find detours around potential voids. A simple algorithm for finding detours around voids is to switch to broadcasting when approaching voids regions. Other measures to avoid void generally require that information is exchanged between the nodes. In the depth-based approach suggested in [31], the node examines its neighbors to check whether they can provide

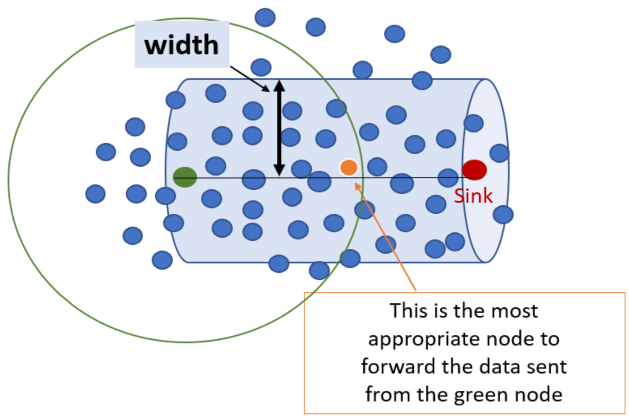

Figure 6. Time slotted communication. TDMA

positive progress toward the destination. If not, the node requests information from two-hop nodes to adjust its depth such that positive forwarding can be resumed. To reduce the void problem, and improve the Packet Delivery Ratio (PDR), a holding-time that takes several factors into consideration is suggested in [32]. Firstly, a reliability index is calculated based on the energy of the current node and the energy of the forwarding region. In order to limit formation of energy holes and thereby increase the reliability, the forwarding region with the highest energy is selected. Secondly, an advancement factor is used: The depth of the node is calculated so that a small decrease in the depth gives an exponential increase in priority. This reduces the probability of duplicate packet transmissions because the priority difference is significant, even for a low change in depth. Third, a shortest path index is used. It combines the number of hops toward the destination and the average depth of the nodes in the next hop.

Other well-known algorithms used in terrestrial Wireless Sensor Networks (WSNs) to reduce broadcasting, such as probabilistic and counter-based schemes may be well-worth testing in underwater environments. Counter-based schemes are based on the fact that broadcasting a message that has already been broadcasted by several neighboring nodes will not substantially increase the area covered. Thus, the nodes are prevented from rebroadcasting messages if the expected additional coverage is limited. Basically, the nodes count the number of times a message is received while waiting for medium access. If the counter becomes higher than a threshold, the transmission is canceled, otherwise the message is transmitted [33]. The method is applied in the Dflood algorithm suggested in [34, 35]. An alternative "gossiping" approach to reduce the broadcasting is introduced in [36].

In probabilistic schemes, the nodes will rebroadcast messages with a probability P. If P = 1 the data packets are broadcasted. There is a certain probability that no neighbors choose to forward a packet. To ensure the progress of a packet towards the destination, the sender can re-emit the packet if no forwarded packets are heard. However, to ensure the packet's progress, the sender may need to re-emit the packet several times, which increases network traffic. In addition, the packet may have been forwarded by nodes connected over a unidirectional link, which means that the re-emitted packets are a waste of both energy and bandwidth.

An alternative to broadcasting may be repeated transmission of every packet. This solution is used in [37], where nodes repeatedly transmit the same packet to increase the probability of successful packet reception. The wanted success probability decides the number of repetitions. No acknowledgement or channel reservation is used. The disadvantage of this method is that both bandwidth and energy are wasted for all packet transmissions that appear after the packet is successfully received. An advantage, however, is the constraining of the interference area that each packet generates when transmitted. Broadcasting means that dispersed neighboring nodes, all with different coverage areas, forward the same packet. Thus, a larger area is affected by the transmission, i.e., the interference area increases. This reduces the probability that packets, generated by nodes located in a different part of the network, are successfully received.

To summarize, due to dynamically changing channel conditions and long propagation delays in the underwater environment, broadcasting may be a better solution than reusing terrestrial routing protocols that generate specific routing paths. Broadcast-based forwarding is likely to improve the probability of packets reaching their intended destination. However, the broadcasting procedure should be constrained to reduce both energy consumption and network traffic.

V. OTHER SOLUTIONS USED IN TERRESTRIAL COMMUNICATION

Software Defined Network (SDN) is a technology aimed at enabling efficient and dynamic network configuration to improve network performance [38, 39]. This is done by centralizing the network management, implement it in software, and base it on complete network information combined with knowledge of the requirements put forward by the running applications. The SDN architecture is generally divided into three layers, application, control, and data layer. The programs at the application layer informs the control layer of desired network behavior and requirements. The control plane manages and dictates how the data plane should handle data traffic. In addition, it can monitor the traffic flow and resource utilization to dynamically manage the network configuration to improve the performance according to the request sent by the application layer. The data layer concerns the actual data forwarding that takes place at the distributed network devices, i.e., routers and switches.

Using SDN in USWN raises challenges. Control messages between the network nodes and the central controller are often transmitted on a secure channel, which requires reliable communication guaranteed by IP-based end-to-end connections. The dynamic channel quality in the underwater environment makes it difficult to support such guarantees. Other challenges relate to availability, performance, and security. The central controller must be available, which is not always the case in underwater communication. To maintain network performance, varying channel conditions, varying traffic load, and requests must be handled within time limits that are short enough to follow the dynamically changing characteristics of the underwater environment. The controller must be secured to ensure that only authorized applications are able to modify the network configuration, although, some security functions can also be improved since centralized SDN may efficiently protect against malicious attacks by monitoring and detecting irregular behavior [40].

Another software-related solution is to use Machine Learning (ML), whose algorithms can generally be divided into three categories: supervised, unsupervised and reinforcement learning (RL) [41, 42]. In supervised learning a training set of defined input parameters gives a set of known output parameters. These parameters are used to generate a system model employing the learned relationship between input, output and system parameters. The objective is to predict the correct output vector for a given input vector. Unsupervised learning means that no targets outputs are provided. The objective is to discover a useful representation of the input data. Examples of criterions for learning can be maximization of output variance [43], or to identify suitable clusters based on similarities of the input samples [42]. RL deals with the ability to learn the mapping from situation to actions so as to maximize the long-term reward. The goal is to learn through experience, i.e., decide which action yields the highest reward by trying them [44]. This means that RL algorithms dynamically optimize processes, and is therefore a frequently suggested algorithm for underwater communication [45]. A common approach for RL is Q-learning [45], which is described as a Markov Decision Process (MDP) that handles problems as random transitions and rewards. Under the environment of the current state, a software agent performs an action that with a given probability makes the agent transition to a new state [46]. The state transitions return some positive or negative reward, and the goal for the agent is to find a policy that will maximize rewards over time. Q-value pertain to the total rewards the agent can expect if it acts optimally.

An important issue with Q-learning is that it does not scale when there are too many actions or states [45, 47]. A solution to save space and time is to use deep Q-network (DQN), where deep neural network (DNN) is used to estimate Q-values. The DQN is trained to predict Q-values using supervised learning. The state is the input and an estimated Q-value for each possible action is the output. Thus, Q-learning is combined with DNN to save space and time.

Using ML means that several parameters can be taken into account, and the solutions can be more adaptable to changing environments. In [48] both latency, energy, globally optimal paths, and mobility are taken into consideration using a ML approach where reinforcement learning is combined with neural network. The suggested protocol is called Deep Q-network-based energy and latency-aware routing protocol (DQELR). In [49] RL is used to take energy consumption, channel condition, and number of retransmissions left before discarding the packet into consideration to select the set of next-hop nodes among its neighbors. The set can consist of everything from one to all neighboring nodes depending on whether the aim is to reduce energy consumption or maximizing transmission reliability. Overhearing is used to verify that transmitted packets are further relayed by at least one next-hop node. To account for link asymmetry, the nodes take into account both that the packet they transmit to their next-hop nodes can be lost, and that they may fail to overhear the packets when they are retransmitted. The suggested protocol is called Channel-aware Reinforcement learning-based Multi-path Adaptive routing (CARMA). Compared against a hop-count routing protocol as well as flooding, the simulations in [49] shows that, as expected, transmission along several paths increase protocol robustness. However, the PDR is substantially reduced when flooding is used in large network with high traffic. Thus, it is concluded that dynamically changing the number of relays is advantageous. Experimental at sea measurements underline poor and varying link quality, and also demonstrate that links are often asymmetric. Transmission through several next-hop neighbours as done using CARMA, improves the PDR under these conditions.

The high propagation delay of underwater environment means that the implicit assumption in RL: that the feedback/ reward is immediately presented to the agent, is not valid. To address this limitation, X. Ye et al. [50] suggest a deep reinforcement learning (DRL) algorithm that takes an action regardless of whether the reward of previous step has been received yet or not. The algorithm is called delayed-reward deep Q-network (DR-DQN). No time is wasted to wait for a new reward. Through a series of observation-action-reward the agent learns to fully exploit the timeslots that may otherwise be wasted due to transmission delay. Using the DR-DQN method, a deep-learning multiple access protocol is presented (DR-DRMA). DNN is used to predict the action-values in Q-learning. To reduce the energy consumption of the nodes, the DNN is trained only if the average reward exceeds a threshold.

One of the great advantages of using ML is that it creates a very autonomous network, where protocol choices and solutions adapt to the current state of the environment. However, troubleshooting can be challenge when using ML. Physical inspection of the nodes and environment is generally unfeasible. Machine learning may generate complex relations between the input parameters and output parameters. Thus, it is not always easy to decide which output to expect for a given set of input parameters. This uncertainty complicates troubleshooting since it is challenging to decide whether the unexpected network behavior is caused by poorly designed ML algorithms or physical/environmental characteristics.

VI. OPEN RESEARCH CHALLENGES

In this section, we pinpoint some topics for further studies based on contemplating the characteristics of underwater modems and the environment. The characteristics are presented in Table 2. Some of the entries in the table are represented as a range of values. These are values reported in [51], where several commercial as well as research modems are investigated.

Starting with power consumption, it is observed that transmission power is generally higher than power consumed for receiving. Looking at the data for each individual modem in [51] reveals that the ratio of transmission power consumption to receiving power consumption is between 1.4 and 188, and for the majority of the modems the ratio is between 10-100. In addition, the power consumed in sleep mode is generally lower than for receiving, the ratio of receiving to sleep mode is from about 1.7 over 1000. To reduce energy and lengthen the network lifetime solutions that focus on reducing the transmission time and enables nodes to enter sleep mode should be studied. Sleep protocols are extensively studied for terrestrial WSNs [52-54], and there are probably ideas that can be adapted for underwater communication. Reducing transmission time can be realized for instance by using overhearing to learn traffic patterns to prevent collisions, and/or use advanced ML techniques to predict channel conditions to decide when to transmit, and to decide the most efficient transmission strategy, for instance whether to use unicast, multicast, broadcast.

Regarding the low propagation speed, it is recommended to study receiver-centric approaches to avoid collisions. Furthermore, due to the low data rate, approaches that avoid spending bandwidth on unnecessary data should be studied. Statistical methods and aggregation, or more intelligent approaches based on ML, could be used in this regard.

Finally, increasing the frequency increases the data rate and reduces the transmission range. Higher data rates can increase the amount of information exchanged, or can be used to reduce the duration of the packets to reduce the collision probability.

VII. Conclusion

MAC and network layer solutions for underwater communication require that characteristics such as long propagation delay, dynamic channel characteristic, and limited bandwidth are considered. Long delays are especially challenging for MAC protocols. The time available for access control is reduced, and the limited channel resources should not be depleted by large amounts of management traffic. For efficient utilization of the limited channel capacity, the focus should be on solutions that both reduce the time between received packets, and, at the same time, prevent packet collisions at the receiver.

Table 2 Modem and environments characteristics [51, 55].

Parameter	Value
Propagation speed	$1.5*10^3$ m/s
Datarate	In the order of kbps, increases with inreased frequency.
Transmissoin range	50m- 10km, reduced with increased frequency
Transmission power	1-40W Commercial, 0.1-120 W Research
Receiving power	0.6-1.8W Commercial, 0.02-1.2 W Research
Standby	0.0005-0.6W Commercial, 20-60mW Research
Sleep	In the order of mW.

Dynamic channel properties make it challenging to generate fixed routes. To reduce the probability of packets being lost during forwarding, we recommend to use constrained broadcasting techniques. Location-based techniques seem to be especially promising.

Machine learning techniques should be further investigated to improve networks' ability to dynamically adapt to the changing characteristics of the underwater environment.

In future work, promising solutions will be selected for further investigations and experimental testing in an underwater test facility at the west-coast of Norway.

Acknowledgment

The work is funded by the SFI Smart Ocean NFR Project 309612/F40.

References

[1] A.-L. Kampen, "Protocols for Underwater Wireless Sensor Networks-Challenges and Solutions," in The Fifteenth International Conference on Sensor Technologies and Applications, SENSORCOMM. International Academy, Research and Industry Association (IARIA), pp. 34-40, 2021.

[2] United Nations, Sustainable Development. "Goal 14." United Nations. https://sdgs.un.org/goals/goal14 (retrieved: May 2022).

[3] C. M. Gussen, P. S. Diniz, M. Campos, W. A. Martins, F. M. Costa, and J. N. Gois, "A survey of underwater wireless communication technologies," J. Commun. Inf. Sys, vol. 31, no. 1, pp. 242-255, 2016.

[4] S. Gauni, C. Manimegalai, K. M. Krishnan, V. Shreeram, V. Arvind, and T. N. Srinivas, "Design and Analysis of Co-operative Acoustic and Optical Hybrid Communication for Underwater Communication," Wireless Personal Communications, vol. 117, no. 2, pp. 561-575, 2021.

[5] E. Zanaj, E. Gambi, B. Zanaj, D. Disha, and N. Kola, "Underwater wireless sensor networks: Estimation of acoustic channel in shallow water," Applied Sciences, vol. 10, no. 18, p. 6393, 2020.

[6] S. Jiang, "State-of-the-art medium access control (MAC) protocols for underwater acoustic networks: A survey based on a MAC reference model," IEEE communications surveys & tutorials, vol. 20, no. 1, pp. 96-131, 2017.

[7] A. Al Guqhaiman, O. Akanbi, A. Aljaedi, and C. E. Chow, "A survey on MAC protocol approaches for underwater wireless sensor networks," IEEE Sensors Journal, vol. 21, no. 3, pp. 3916-3932, 2020.

[8] A. Boukerche and P. Sun, "Design of Algorithms and Protocols for Underwater Acoustic Wireless Sensor Networks," ACM Computing Surveys (CSUR), vol. 53, no. 6, pp. 1-34, 2020.

[9] S. Khisa and S. Moh, "Survey on Recent Advancements in Energy-Efficient Routing Protocols for Underwater Wireless Sensor Networks," IEEE Access, vol. 9, pp. 55045-55062, 2021.

[10] M. Khalid et al., "A survey of routing issues and associated protocols in underwater wireless sensor networks," Journal of Sensors, vol. 2017, 2017.

[11] Q. Lu and J. Shengming, "A review of routing protocols of underwater acoustic sensor networks from application perspective," in 2016 IEEE International Conference on Communication Systems (ICCS), IEEE, pp. 1-6, 2016.

[12] M. Ayaz, I. Baig, A. Abdullah, and I. Faye, "A survey on routing techniques in underwater wireless sensor networks," Journal of Network and Computer Applications, vol. 34, no. 6, pp. 1908-1927, 2011.

[13] N. Li, J.-F. Martínez, J. M. Meneses Chaus, and M. Eckert, "A survey on underwater acoustic sensor network routing protocols," Sensors, vol. 16, no. 3, p. 414, 2016.

[14] H. Karl and A. Willig, Protocols and architectures for wireless sensor networks. John Wiley & Sons, 2007.

[15] A. A. Syed and J. S. Heidemann, "Time Synchronization for High Latency Acoustic Networks," in Infocom, vol. 6, pp. 1-12, 2006.

[16] W.-H. Liao and C.-C. Huang, "SF-MAC: A spatially fair MAC protocol for underwater acoustic sensor networks," IEEE sensors journal, vol. 12, no. 6, pp. 1686-1694, 2011.

[17] M. A. Hossain, A. Karmaker, and M. S. Alam, "Resolving spatial unfairness problem with reduced-handshaking in underwater acoustic sensor network," in 2017 International Conference on Wireless Communications, Signal Processing and Networking (WiSPNET), IEEE, pp. 2178-2182, 2017.

[18] K. Kebkal, A. Mashoshin, and N. Morozs, "Solutions for underwater communication and positioning network development," Gyroscopy and navigation, vol. 10, no. 3, pp. 161-179, 2019.

[19] N. Chirdchoo, W.-S. Soh, and K. C. Chua, "RIPT: A receiver-initiated reservation-based protocol for underwater acoustic networks," IEEE Journal on Selected Areas in Communications, vol. 26, no. 9, pp. 1744-1753, 2008.

[20] R. Petroccia, C. Petrioli, and J. Potter, "Performance evaluation of underwater medium access control protocols: At-sea experiments," IEEE Journal of Oceanic Engineering, vol. 43, no. 2, pp. 547-556, 2017.

[21] A. A. Syed, W. Ye, and J. Heidemann, "T-Lohi: A new class of MAC protocols for underwater acoustic sensor networks," in IEEE INFOCOM 2008-The 27th Conference on Computer Communications, IEEE, pp. 231-235, 2008.

[22] A. A. Syed, W. Ye, and J. Heidemann, "Comparison and evaluation of the T-Lohi MAC for underwater acoustic sensor networks," IEEE Journal on Selected Areas in Communications, vol. 26, no. 9, pp. 1731-1743, 2008.

[23] C. Zidi, F. Bouabdallah, R. Boutaba, and A. Mehaoua, "MC-UWMAC: A multi-channel MAC protocol for underwater sensor networks," in 2017 International Conference on Wireless Networks and Mobile Communications (WINCOM), IEEE, pp. 1-6, 2017.

[24] F. Bouabdallah, R. Boutaba, and A. Mehaoua, "Collision avoidance energy efficient multi-channel MAC protocol for underwater acoustic sensor networks," IEEE Transactions on Mobile Computing, vol. 18, no. 10, pp. 2298-2314, 2018.

[25] Z. Zhou, Z. Peng, J.-H. Cui, and Z. Jiang, "Handling triple hidden terminal problems for multichannel MAC in long-delay underwater sensor networks," IEEE Transactions on Mobile Computing, vol. 11, no. 1, pp. 139-154, 2011.

[26] W. Liu et al., "APOLL: Adaptive polling for reconfigurable underwater data collection systems," in 2018 OCEANS-MTS/IEEE Kobe Techno-Oceans (OTO), IEEE, pp. 1-9, 2018.

[27] N. Morozs, P. Mitchell, and Y. V. Zakharov, "TDA-MAC: TDMA without clock synchronization in underwater acoustic networks," IEEE Access, vol. 6, pp. 1091-1108, 2017.

[28] V. G. Menon and P. J. Prathap, "Comparative analysis of opportunistic routing protocols for underwater acoustic sensor networks," in 2016 international conference on emerging technological trends (ICETT), IEEE, pp. 1-5, 2016.

[29] S. Lee and D. Kim, "Underwater hybrid routing protocol for UWSNs," in 2013 Fifth International Conference on Ubiquitous and Future Networks (ICUFN), IEEE, pp. 472-475, 2013.

[30] S. M. Mazinani, H. Yousefi, and M. Mirzaie, "A vector-based routing protocol in underwater wireless sensor networks," Wireless Personal Communications, vol. 100, no. 4, pp. 1569-1583, 2018.

[31] R. W. Coutinho, A. Boukerche, L. F. Vieira, and A. A. Loureiro, "Geographic and opportunistic routing for underwater sensor networks," IEEE Transactions on Computers, vol. 65, no. 2, pp. 548-561, 2015.

[32] M. Ismail et al., "Reliable path selection and opportunistic routing protocol for underwater wireless sensor networks," IEEE Access, vol. 8, pp. 100346-100364, 2020.

[33] Y.-C. Tseng, S.-Y. Ni, Y.-S. Chen, and J.-P. Sheu, "The broadcast storm problem in a mobile ad hoc network," Wireless networks, vol. 8, no. 2, pp. 153-167, 2002.

[34] R. Otnes and S. Haavik, "Duplicate reduction with adaptive backoff for a flooding-based underwater network protocol," in 2013 MTS/IEEE OCEANS-Bergen, IEEE, pp. 1-6, 2013.

[35] R. Otnes, P. A. van Walree, H. Buen, and H. Song, "Underwater acoustic network simulation with lookup tables from physical-layer replay," IEEE Journal of Oceanic Engineering, vol. 40, no. 4, pp. 822-840, 2015.

[36] M. Goetz and I. Nissen, "GUWMANET—Multicast routing in underwater acoustic networks," in 2012 military communications and information systems conference (MCC), IEEE, pp. 1-8, 2012.

[37] C. Li, Y. Xu, C. Xu, Z. An, B. Diao, and X. Li, "DTMAC: A delay tolerant MAC protocol for underwater wireless sensor networks," IEEE Sensors Journal, vol. 16, no. 11, pp. 4137-4146, 2015.

[38] H. Luo, K. Wu, R. Ruby, Y. Liang, Z. Guo, and L. M. Ni, "Software-defined architectures and technologies for underwater wireless sensor networks: A survey," IEEE Communications Surveys & Tutorials, vol. 20, no. 4, pp. 2855-2888, 2018.

[39] R. Ruby, S. Zhong, B. M. ElHalawany, H. Luo, and K. Wu, "SDN-enabled energy-aware routing in underwater multi-modal communication networks," IEEE/ACM Transactions on Networking, vol. 29, no. 3, pp. 965-978, 2021.

[40] S. Jiang, "On securing underwater acoustic networks: A survey," IEEE Communications Surveys & Tutorials, vol. 21, no. 1, pp. 729-752, 2018.

[41] M. S. Mahdavinejad, M. Rezvan, M. Barekatain, P. Adibi, P. Barnaghi, and A. P. Sheth, "Machine learning for Internet of Things data analysis: A survey," Digital Communications and Networks, vol. 4, no. 3, pp. 161-175, 2018.

[42] M. A. Alsheikh, S. Lin, D. Niyato, and H.-P. Tan, "Machine learning in wireless sensor networks: Algorithms, strategies, and applications," IEEE Communications Surveys & Tutorials, vol. 16, no. 4, pp. 1996-2018, 2014.

[43] P. F. Baldi and K. Hornik, "Learning in linear neural networks: A survey," IEEE Transactions on neural networks, vol. 6, no. 4, pp. 837-858, 1995.

[44] W. G. Hatcher and W. Yu, "A survey of deep learning: Platforms, applications and emerging research trends," IEEE Access, vol. 6, pp. 24411-24432, 2018.

[45] R. T. Rodoshi, Y. Song, and W. Choi, "Reinforcement Learning-Based Routing Protocol for Underwater Wireless Sensor Networks: A Comparative Survey," IEEE Access, vol. 9, pp. 154578-154599, 2021.

[46] S. K. Sharma and X. Wang, "Toward massive machine type communications in ultra-dense cellular IoT networks: Current issues and machine learning-assisted solutions," IEEE Communications Surveys & Tutorials, vol. 22, no. 1, pp. 426-471, 2019.

[47] H. Li, H. Gao, T. Lv, and Y. Lu, "Deep Q-learning based dynamic resource allocation for self-powered ultra-dense networks," in 2018 IEEE International Conference on Communications Workshops (ICC Workshops), IEEE, pp. 1-6, 2018.

[48] Y. Su, R. Fan, X. Fu, and Z. Jin, "DQELR: An adaptive deep Q-network-based energy-and latency-aware routing protocol design for underwater acoustic sensor networks," IEEE Access, vol. 7, pp. 9091-9104, 2019.

[49] V. Di Valerio, F. L. Presti, C. Petrioli, L. Picari, D. Spaccini, and S. Basagni, "CARMA: Channel-aware reinforcement learning-based multi-path adaptive routing for underwater wireless sensor networks," IEEE Journal on Selected Areas in Communications, vol. 37, no. 11, pp. 2634-2647, 2019.

[50] X. Ye, Y. Yu, and L. FU, "Deep reinforcement learning based MAC protocol for underwater acoustic networks," IEEE Transactions on Mobile Computing, 2020.

[51] M. Y. I. Zia, J. Poncela, and P. Otero, "State-of-the-art underwater acoustic communication modems: Classifications, analyses and design challenges," Wireless Personal Communications, vol. 116, no. 2, pp. 1325-1360, 2021.

[52] M. A. Jamshed, K. Ali, Q. H. Abbasi, M. A. Imran, and M. Ur-Rehman, "Challenges, applications and future of wireless sensors in Internet of Things: A review," IEEE Sensors Journal, 2022.

[53] J. Singh, R. Kaur, and D. Singh, "A survey and taxonomy on energy management schemes in wireless sensor networks," Journal of Systems Architecture, vol. 111, p. 101782, 2020.

[54] A. Kumar, M. Zhao, K.-J. Wong, Y. L. Guan, and P. H. J. Chong, "A comprehensive study of iot and wsn mac protocols: Research issues, challenges and opportunities," IEEE Access, vol. 6, pp. 76228-76262, 2018.

[55] H. Khan, S. A. Hassan, and H. Jung, "On underwater wireless sensor networks routing protocols: A review," IEEE Sensors Journal, vol. 20, no. 18, pp. 10371-10386, 2020.

Batteryless, Contactless, and Wireless Power Factor and Apparent Power Sensor Using Piezoelectric Film

Short paper

Takaya Yoshitake
Department of Communication Engineering and Informatics
The University of Electro-Communications
Chofu, Japan
Email: y2131168@edu.cc.uec.ac.jp

Shunkichi Takamatsu, Shinichiro Mito
Department of electronic engineering
National Institute of Technology, Tokyo College
Hachioji, Japan
Email: mito@tokyo-ct.ac.jp

***Abstract*—Power measurement of individual machines is required in factories for production control and energy conservation. Therefore, a power consumption monitoring sensor that can be easily retrofitted and requires minimal maintenance should be devised. In this study, we developed a contactless, wireless, and battery less alternating current (AC) apparent power and power factor sensor, wherein a current-sensing transformer serves not only as a noncontact current sensor but also as a power supply for the sensor. The AC voltage waveform was measured without a metal contact by using a piezoelectric film. A low-power circuit was designed to manage the power and measure the power factor from current and voltage waveforms. The prototyped sensor was tested in the factory. The data obtained by the field test were consistent with the results obtained from a commercially available power meter. The developed sensor can enable energy savings and carbon dioxide reduction in industrial applications.**

Keywords-electrical power sensing; electric field; noncontact measurement; energy harvesting; SDG.

I. INTRODUCTION

This study expands on a previous conference submission [1]. The reduction of electrical power consumption remains a pertinent issue in factories with regard to reducing manufacturing costs and CO_2 emissions [2][3] so as to ensure compliance with the International Organization for Standardization (ISO) 14001 standard [4]. Therefore, precise measurement of the power consumption of each unit of equipment is critical [5].

Such measurement requires compact, easy-to-install, and inexpensive wireless power sensors. However, existing sensors cannot satisfy these demands [6]–[11].

To measure the current and voltage waveforms without invading the cables, the development of sensors that can be easily retrofitted. Current waveforms can be easily measured using a commercially available split-type current transformer [12]. Current transformers output an induced current that is proportional to the current flowing in the cable to be measured. This current can be used for sensing and power generation for energy harvesting [13]–[16]. Energy-harvesting batteryless operation considerably reduces maintenance costs. However, noninvasive measurement of the voltage waveform is difficult. Several nonmetallic contact methods for voltage waveform measurement have been proposed [17]–[20] to realize ease of installation and noninvasive measurement. However, these methods are expensive and require multiple probes, which renders implementation difficult.

In this study, we developed a non-metal-contact voltage measurement method based on a single probe using a piezoelectric film. Furthermore, we fabricated and evaluated an energy-harvesting, noninvasive, and retrofittable wireless power consumption sensor that consists of the proposed voltage sensor, a current transformer, an energy-harvesting circuit, a power factor (PF) measurement circuit, and a wireless communication module for use in factories. The device does not require complex electrical circuitry and costs approximately $20 because of its simple design.

In Section 2, a block diagram of the proposed sensor is presented. Section 3 describes the nonmetal contact voltage measurement process using a piezoelectric film. Section 4 presents the power management and PF measurement circuit. Section 5 presents the results of field tests. Finally, Section 6 presents the conclusions of this study.

II. SENSOR CONFIGURATION

The configuration of the developed sensor is illustrated in Figure 1. A current transformer was used to measure the current in a contact-free manner. The operating power of the wireless module can be obtained from the current transformer. The sensor can be powered through energy harvesting. The apparent power was calculated by multiplying the assumed-to-be-constant voltage with the measured current. The PF was calculated using the phase difference between the voltage waveform acquired by the proposed voltage sensor and the current waveform. The obtained apparent power and PF were transmitted using a wireless module (TWE-Lite, Mono Wireless Inc., Kanagawa, Japan).

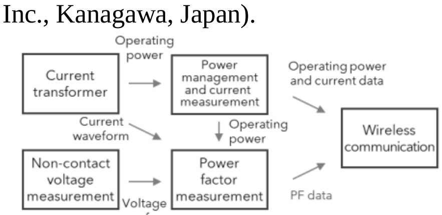

Figure 1. Block diagram of the proposed power factor (PF) and apparent power sensor.

Installation of the developed sensor is easy because noncontact single probes are used for both current and voltage measurements. Furthermore, our sensor requires lower maintenance than conventional sensors because of its energy harvesting-based operation.

III. NON-METAL-CONTACT VOLTAGE MEASUREMENT USING PIEZOELECTRIC FILMS

A. Principle

A piezoelectric film was attached to an electric cable. A cross-sectional view of the cable and piezoelectric film is displayed in Figure 2. The cable was assumed to be a sufficiently long conductor cylinder. When a voltage was applied to the cable, an electric field, *E*, is generated, and a potential difference is created between the nearby electrode pair of the piezoelectric film. The potential difference $v_p(t)$ can be calculated as follows:

$$v_p(t) = -\int_r^{r+a} E\, dr = \frac{q(\mathrm{t})}{2\pi\varepsilon_0\varepsilon_r} \ln\frac{r+a}{r} \quad (1)$$

In Equation (1), *r* is a distance between the center of the cable to a nearest electrode, *a* is a thickness of the dielectric film, and q(t) is the charge per unit length of the cable.

Energized cables and grounded cables have capacitance. Therefore, the voltage applied to cable v(t) and the charge per unit length of cable q(t) have the following relationship:

$$q(t) = Cv(t) \quad (2)$$

where *C* is the capacitance formed between the cables, which is extremely small. Combining the two equations, the relationship between the potential difference v_p(t) and cable voltage v(t) can be expressed as follows:

$$v_p(t) = \frac{Cv(t)}{2\pi\varepsilon_0\varepsilon_r} \ln\frac{r+a}{r} \quad (3)$$

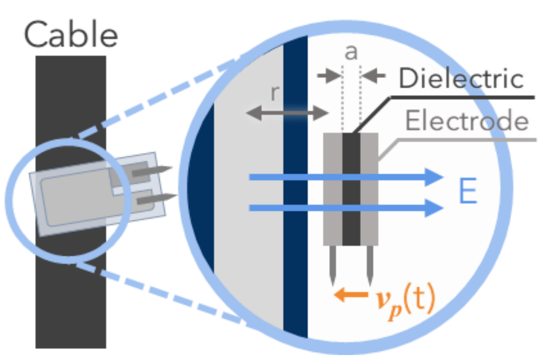

Figure 2. Cross-sectional view of the cable and piezoelectric film

If the piezoelectric film is placed near the cable and *r* is small, the output voltage v_p(t) has a sufficient value for measurement, and it correlates with cable voltage v(t). Therefore, the voltage can be measured without a metal contact. Equation (3) indicates that the output voltage v_p(t) is proportional to the thickness of the piezoelectric film.

However, the output of the piezoelectric film depends on the distance.

B. Prototyping

Noninvasive voltage measurement can be realized using by measuring the electric field strength around a wire using a single probe when the voltage is applied to the wire [17][18]. We used piezoelectric films to realize a low-cost electric field measurement method. Piezoelectric films comprise a piezoelectric material sandwiched between metal electrodes. The piezoelectric material was polarized by the electric field around the wire, and a potential difference was generated between the two electrodes. Thus, the electric field around the wire could be detected using a single piezoelectric probe.

A non-metal-contact voltage probe was prototyped, as displayed in Figure 3. A commercially available piezoelectric film (LDT0-028K, TE Connectivity, Schaffhausen, Switzerland) was bent and placed at a uniform distance from the center of the wire. The sensor frame was fabricated using a 3D printer (UP BOX Plus, Beijing Tiertime Technology Co. Ltd., Beijing, China). The cable-side electrode was set as positive.

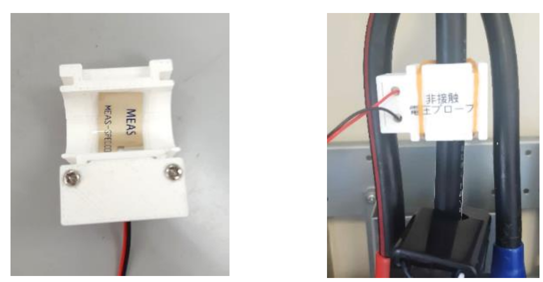

(a) (b)

Figure 3. (a) Fabricated non-metal-contact voltage probe. (b) Probe placed on the electric cable.

C. Measurement

The voltage waveform observed using the probe is displayed in Figure 4. Although the output voltage and phase varied with the distance between the piezoelectric film and the wire, the correlation coefficient obtained for the actual and measured waveforms was 0.99. The proposed method can measure the relative change in the voltage, which is sufficient to enable PF calculation. The piezoelectric sensor output was related to the actual voltage and was consistent with the calculation results from the equivalent circuit. Furthermore, the output was almost zero when the neutral side of the cable was measured, which indicated that hum noise was not measured.

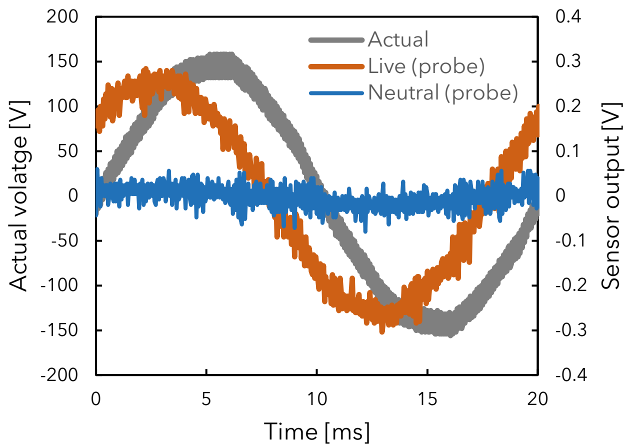

Figure 4. Results of non-metal-contact voltage measurements using the piezoelectric film. The piezoelectric sensor output was related in advance to the actual voltage. The neutral side output is almost zero.

D. *Linearity of the output for the applied electric field*

To evaluate the probe characteristics against the voltage applied to the cable, we measured the relationship between the applied electric field strength and output. A conductive tape was attached to both sides of the piezoelectric film, and a signal generator was used to apply voltage to the tape. The results displayed in Figure 6 confirmed that the output was linear with respect to the applied electric field. The inclination was slightly larger at higher frequencies.

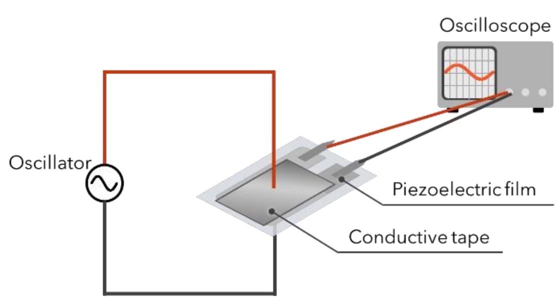

Figure 5. Evaluation of the probe characteristics for the applied electric field.

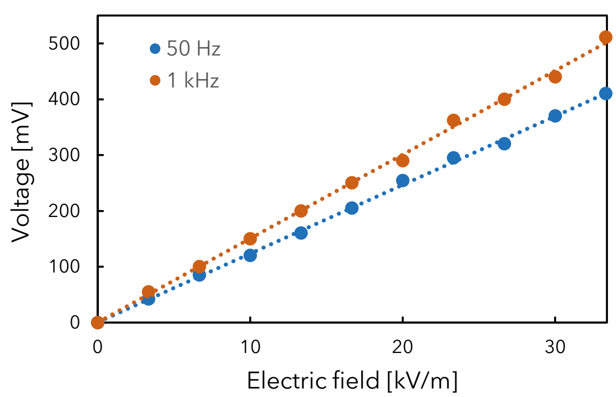

Figure 6. Output voltage of the probe for electric field intensity. Output has linearity to the applied electric field.

E. *Frequency response*

The frequency response of the output of the fabricated probe was measured. The voltage of the measured cable was 100 V_{rms} for all frequencies. The obtained frequency characteristics are displayed in Figure 8. The gain reference was set to the output at 350 Hz. The cutoff frequency was 25 Hz, which indicated excellent low-frequency characteristics.

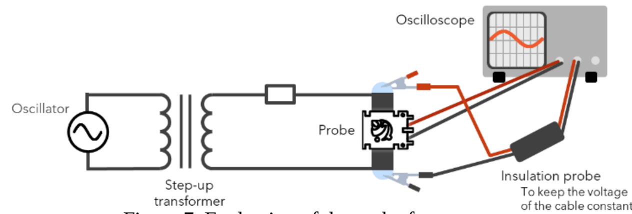

Figure 7. Evaluation of the probe frequency response.

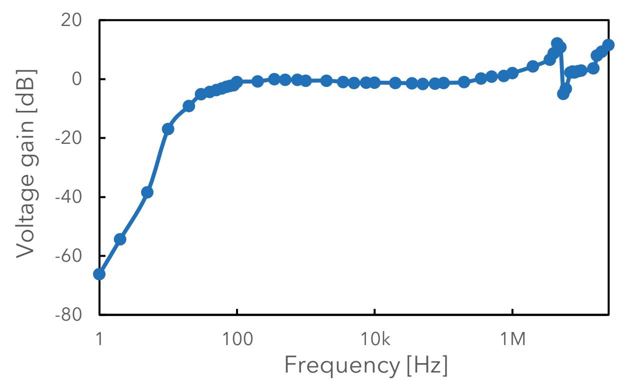

Figure 8. Frequency response of the voltage measurement by the piezoelectric film. The gain reference was set to the output at 350 Hz. The sensor gain was stable in the range of 80 Hz to 1 MHz and the cutoff frequency was 25 Hz.

IV. CIRCUIT OF THE PROPOSED METHOD

A. *Power management and current measurement circuit*

The power management circuit of the fabricated sensor is illustrated in Figure 9. A current transformer was installed on the cable to be measured, and the current obtained from the transformer was full-wave rectified, smoothed, and measured. The power management circuit outputted not only the operation power for the entire circuit but also the voltage that correlated with the current flowing in the cable.

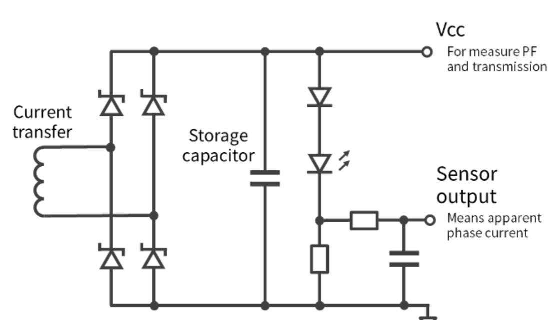

Figure 9. Overview of the power management circuit.

First, we simulated the transient response of the power supply voltage (V_{cc}) of the power management circuit when currents of 1, 5, 10, 20, and 30 A were applied to the measured cable. The circuit used in the simulation is illustrated in Figure 10. Here, C_1, L_1, and R_1 on the primary side of the transformer are the equivalent circuits of the cable. The simulation results for V_{cc} are displayed in Figure 11, which reveals V_{cc} converges after a few seconds. Furthermore, the results revealed that the voltage depended on the amount of current flowing through the cable. Here, V_{cc} was determined by a measurement resistor R_6 (47 Ω) and D_5 and D_6. We confirmed that the operating voltage of a general micro controller (1.8 to 3.6 V) can be obtained in the range 1 to 20 A, where we want to perform the measurement. The measurement range of the current can be modified by changing the resistance value or the threshold of the diodes.

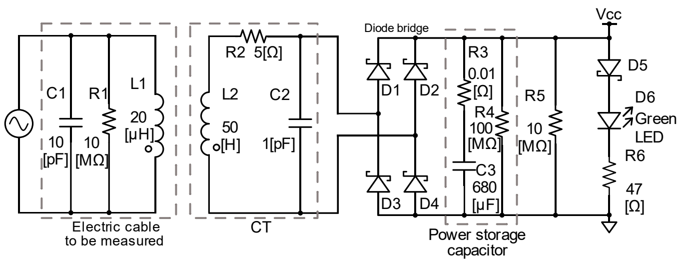

Figure 10. Simulation circuit for the cable current and supply voltage for the sensor.

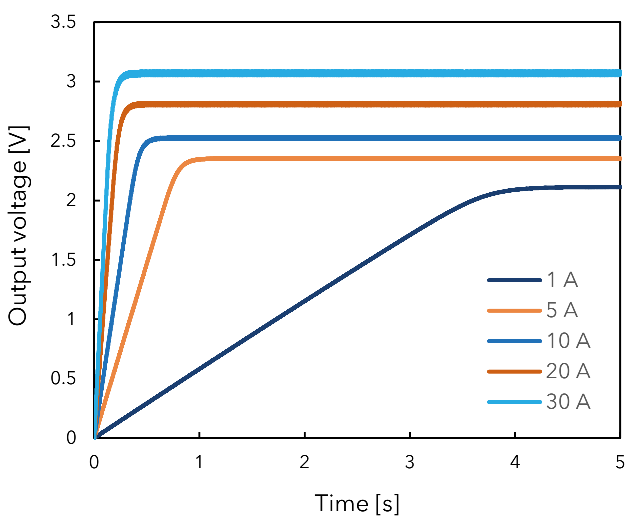

Figure 11. Simulation results of the cable current dependence on the supply voltage (V_{cc}). V_{cc} converges after a few seconds and depends on the amount of current flowing in the cable.

Next, we simulated the relationship between the measured current and the sensor output voltage. The current transformer was assumed to be a current source that outputs current proportional to the current flowing in the cable. The circuit displayed in Figure 12 was simulated.

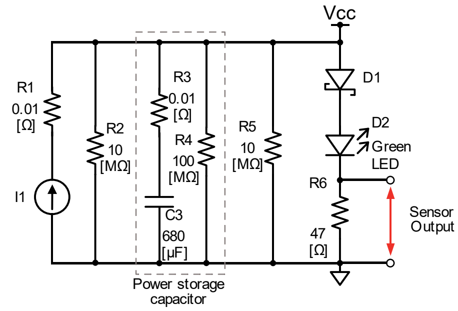

Figure 12. Simulation circuit of the power management circuit with the input current.

The results of the relationship between the current, power supply voltage for our sensor, and the voltage of R_6 are displayed in Figure 13. The supply voltage was rapidly increased to the operating voltage of the microcontroller. However, the sensor output was proportional to the output of the current transformer. The power management circuit simultaneously generated both the power supply and current measurement voltages.

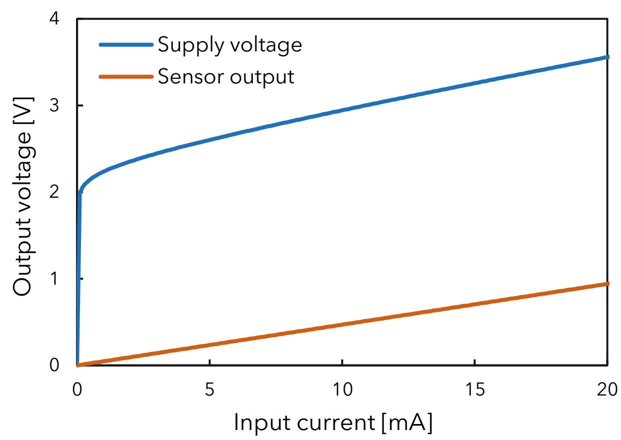

Figure 13. Simulation results of the sensor supply voltage and the sensor output for the input current. The supply voltage rapidly increases to the operation voltage of the micro controller. By contrast, the sensor output is proportional to the output of the current transformer

The sensor output was changed by the power consumption of the microcontroller. The microcontroller sent the data every 5 s and consumed 15 mA for 4 ms to send the data. For the other 4996 ms, the microcontroller was in the sleep mode and consumed 1.5 μA. An RC low-pass filter with a time constant of 1 s was used to reduce the influence of the sending current.

B. PF measurement circuit

The developed sensor was operated using the power obtained from the current transformer; thus, realization of low-power PF measurement was critical. In this study, we used an analog circuit to perform PF measurements with a low power consumption.

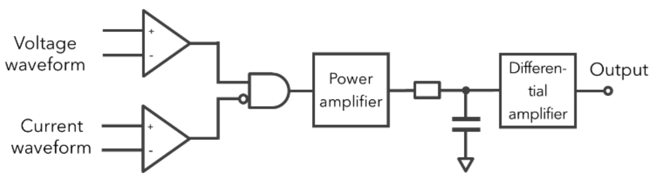

Figure 14. Block diagram of the PF measurement circuit.

Figure 14 displays the block diagram of the fabricated PF measurement circuit. The current and voltage waveforms were converted into square waves, and the phase difference was obtained as the pulse width by calculating the logical product of these waves. Subsequently, the phase difference was output as an analog voltage through the power amplification, smoothing, and differential amplification processes. The output was connected to the analog-to-digital converter of the wireless module, and the data were transmitted. This circuit can be applied to both the single- and three-phase electrical loads.

V. FABRICATION AND FIELD TEST

Noncontact wireless apparent power and PF sensors were fabricated, as displayed in Figure 15. The fabricated sensor was attached to an injection molding machine (SH100C, Sumitomo Heavy Industries, Tokyo, Japan) for field testing (Figure 16).

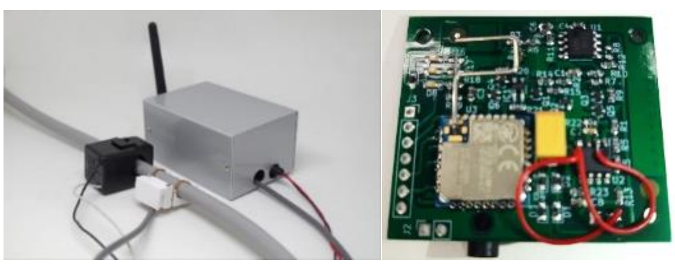

(a) (b)

Figure 15. (a) Fabricated sensor. The black probe is the current transformer, and the white probe is the voltage probe developed in this work. The silver box contains the processing circuit. (b) Fabricated sensor board.

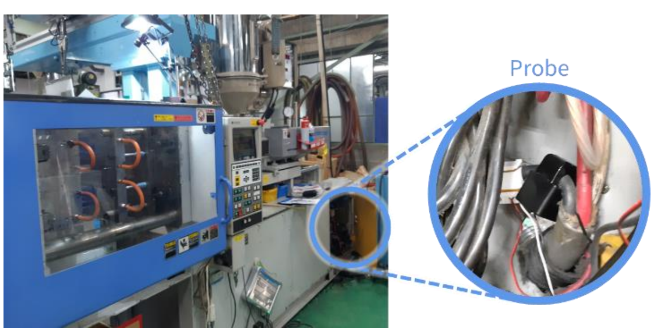

Figure 16. Overview of the field test. The fabricated probes and circuit were applied to the injection molding machine.

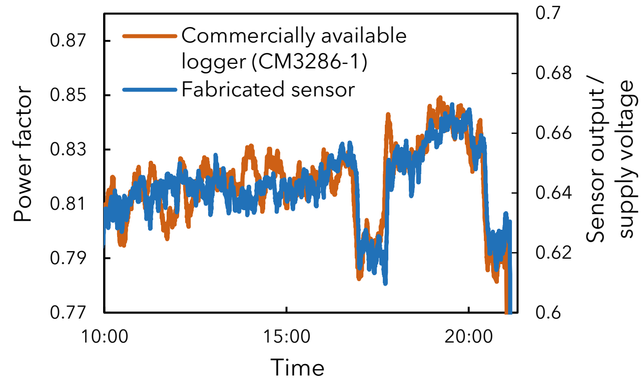

Figure 17. Comparison of the PFs obtained from a commercially available logger and the fabricated sensor.

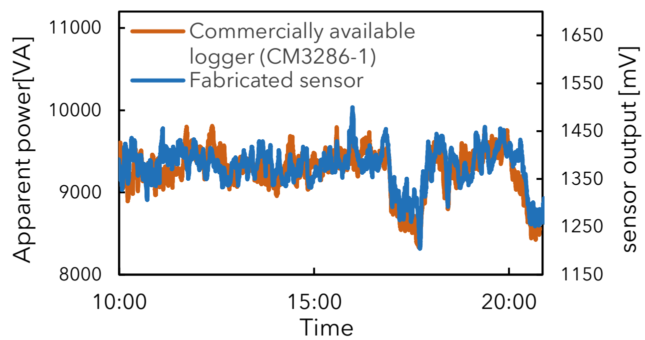

Figure 18. Comparison of the apparent power results obtained from a commercially available logger and the fabricated sensor.

Figures 17 and 18 display comparisons of the PFs and apparent power values, respectively, which were measured using the developed sensor with those measured using a commercially available power logger (CM3286-01, HIOKI E.E., Tokyo, Japan). The PF obtained by the developed sensor had a correlation coefficient of 0.80 with that measured using a commercial logger. Apparent power had a correlation coefficient of 0.73. These results indicate that the proposed sensor can measure the power consumption sufficiently accurately. This accuracy is suitable for rough logging of the PF and can be improved by calibration and grounding processes.

VI. CONCLUSION

Voltage waveforms were measured using a single piezoelectric probe without metal contacts. Novel energy-harvesting wireless apparent power and PF sensors were developed using the piezoelectric probe. The data acquired using the developed sensor were consistent with the data acquired using a commercially available power meter.

ACKNOWLEDGMENT

This research is supported by the Adaptable and Seamless echnology Transfer Program (A-STEP) JPMJTM20M3 from the Japan Science and Technology Agency (JST). We would like to thank Editage (www.editage.com) for English language editing.

References

[1] T. Yoshitake, S. Takamatsu, and S. Mito, "Development and application of an energy harvesting power factor and apparent power sensor" in SENSORCOMM 2021, Athens, Greece, Nov. 2021, pp. 8-10, Accessed: 2022.05.10 [Online]. Available from: https://www.thinkmind.org/index.php?view=article&articleid=sensorcomm_2021_1_20_10010

[2] A. Hawkes, "Estimating marginal CO2 emissions rates for national electricity systems," Energy Policy, vol. 38, pp. 5977-5987, 2010.

[3] T. Unger and E. O. Ahlgren, "Impacts of a common green certificate market on electricity and CO2-emission markets in the Nordic countries," Energy Policy, vol. 33, pp. 2152-2163, 2005.

[4] P. Gupta, "End of life considerations for EV batteries - ISO and Indian business perspectives," 6th Hybrid and Electric Vehicles Conference (HEVC 2016), 2016, pp. 1-5, doi: 10.1049/cp.2016.0989.

[5] W. Gans, A. Alberini, and A. Longo, "Smart meter devices and the effect of feedback on residential electricityconsumption: Evidence from a natural experiment in Northern Ireland," Energy Economics, vol. 36, pp. 729-743, 2013.

[6] B. K. Barman, S. N. Yadav, S. Kumar, and S. Gope, "IOT Based Smart Energy Meter for Efficient Energy Utilization in Smart Grid," 2018 2nd International Conference on Power, Energy and Environment: Towards Smart Technology (ICEPE), 2018, pp. 1-5, doi: 10.1109/EPETSG.2018.8658501.

[7] T. Sirojan, S. Lu, B. T. Phung, and E. Ambikairajah, "Embedded Edge Computing for Real-time Smart Meter Data Analytics," 2019 International Conference on Smart Energy Systems and Technologies (SEST), 2019, pp. 1-5, doi: 10.1109/SEST.2019.8849012.

[8] P. Kumar and U. C. Pati, "IoT based monitoring and control of appliances for smart home," 2016 IEEE International Conference on Recent Trends in Electronics, Information & Communication Technology (RTEICT), 2016, pp. 1145-1150, doi: 10.1109/RTEICT.2016.7808011.

[9] A. S. Musleh, M. Debouza, and M. Farook, "Design and implementation of smart plug: An Internet of Things (IoT) approach," 2017 International Conference on Electrical and Computing Technologies and Applications (ICECTA), 2017, pp. 1-4, doi: 10.1109/ICECTA.2017.8252033.

[10] W. Hlaing et al., "Implementation of WiFi-based single phase smart meter for Internet of Things (IoT)," 2017 International Electrical Engineering Congress (iEECON), 2017, pp. 1-4, doi: 10.1109/IEECON.2017.8075793.

[11] C. Huang, T. Hsien, and G. Jong, "Indoor power meter combined wireless sensor network for smart grid application," 2012 8th International Conference on Information Science and Digital Content Technology (ICIDT2012), 2012, pp. 336-339.

[12] V. Miron-Alexe, "Comparative study regarding measurements of different AC current sensors," 2016 International Symposium on Fundamentals of Electrical Engineering (ISFEE), 2016, pp. 1-6, doi: 10.1109/ISFEE.2016.7803152.

[13] T. L. Companhoni, M. Götz, C. Protasio, and I. Müller, "Development of a Wireless Current Measurement Sensor Node for IoT Applications," 2018 VIII Brazilian Symposium on Computing Systems Engineering (SBESC), 2018, pp. 1-7, doi: 10.1109/SBESC.2018.00010.

[14] T. -C. Huang et al., "120% Harvesting Energy Improvement by Maximum Power Extracting Control for High Sustainability Magnetic Power Monitoring and Harvesting System," in IEEE Transactions on Power Electronics, vol. 30, no. 4, pp. 2262-2274, April 2015, doi: 10.1109/TPEL.2014.2330868.

[15] V. Pavel, Ž. Jiří, K. Jindřich, K. Kamil, S. Jiří, and G. Vjačeslav, "Energy Harvesting and Communication Systems for Power Lines Inspection Robot," 2020 21st International Scientific Conference on Electric Power Engineering (EPE), 2020, pp. 1-4, doi: 10.1109/EPE51172.2020.9269193.

[16] P. Kamat, D. Sutar, and P. Pavan Prasad, "Efficient Energy Harvesting Using Current Tranformer for Smart Grid Application," 2018 2nd International Conference on Trends in Electronics and Informatics (ICOEI), 2018, pp. 343-347, doi: 10.1109/ICOEI.2018.8553892.

[17] D. Onishi et al., "Surface potential measurement of stress grading system of high voltage rotating machine coils using pockels field sensor," 2017 International Symposium on Electrical Insulating Materials (ISEIM), 2017, pp. 95-98, doi: 10.23919/ISEIM.2017.8088697.

[18] C. Peng, P. Yang, X. Wen, D. Fang, and S. Xia, "Design of a novel micromachined non-contact resonant voltage sensor for power distribution systems," SENSORS, 2014 IEEE, 2014, pp. 978-981, doi: 10.1109/ICSENS.2014.6985166.

[19] A. Rodriguez-Garde, A. B. Socorro-Leranoz, M. E. Martinez, J. Goicoechea, and I. R. Matias, "Dynamic Response of Gold-coated Optical Fiber Sensors Subjected to Voltage Variations," 2020 IEEE SENSORS, 2020, pp. 1-4, doi: 10.1109/SENSORS47125.2020.9278838.

[20] P. S. Shenil, R. Arjun, and B. George, "Feasibility study of a non-contact AC voltage measurement system," 2015 IEEE International Instrumentation and Measurement Technology Conference (I2MTC) Proceedings, 2015, pp. 399-404, doi: 10.1109/I2MTC.2015.7151301.